LAWRENCE
LIVERMORE
NATIONAL
LABORATORY

LLNL-JRNL-414527

Corner Turning and Shock Desensitization Experiments plus Numerical Modeling of Detonation Waves in the Triaminotrinitrobenzene Based High Explosive LX-17

C. M. Tarver

July 9, 2009

Journal of Physical Chemistry A

Disclaimer

Corner Turning and Shock Desensitization Experiments plus Numerical Modeling of Detonation Waves in the Triaminotrinitrobenzene Based Explosive LX-17

Craig M. Tarver

Energetic Materials Center, Lawrence Livermore National Laboratory, Livermore, CA 94551

ABSTRACT: Five experiments are presented which test both detonation wave corner turning and shock desensitization properties of the triaminotrinitrobenzene (TATB) based plastic bonded explosive (PBX) LX-17. These experiments used small pentaerythritol tetranitrate (PETN) charges to initiate hemispherical ultrafine TATB (UF TATB) boosters, which then initiated LX-17 hemispherical detonations. The UF TATB boosters were placed under steel shadow plates embedded in the LX-17 cylindrical charges, which were covered by thin aluminum plates. The LX-17 detonation waves propagated outward until they reached the aluminum plates, which were instrumented with timing pins and photonic Doppler velocimetry probes to measure their free surface velocities. X-ray radiographs and framing camera images were taken at various times. The LX-17 detonations propagated around the two corners of the steel shadow plates and into thin LX-17 layers placed between the steel and the top aluminum plates. The detonation waves were met there by weak diverging shocks that propagated through the steel plates and imparted 1 to 2 GPa pressures to these unreacted LX-17 layers. These shock pressures compressed and desensitized the unreacted LX-17, resulting in failures of the LX-17 detonation waves. The hydrodynamics of double corner turning and shock desensitization in the five experiments were modeled in two dimensions using the Ignition and Growth LX-17 detonation reactive flow model. The calculated arrival times and free surface velocity histories of the top aluminum plates were in excellent agreement with the experimental measurements.

INTRODUCTION

Two of the more interesting time dependent solid explosive detonation processes are corner turning and shock desensitization, which is called “dead pressing” in the older literature.[1] The ability of detonation waves to continue to propagate after they encounter abrupt (i. e. 90˚ corners) or more gradual geometry changes (i. e. curved surfaces) is very important to understand in practical explosive charge

design. Shock desensitization occurs when a weak shock wave compresses an explosive charge to full or nearly full density. This greatly reduces the number of voids, which are possible "hot spot reaction sites" upon compression, and makes the charge much less shock sensitive to an oncoming strong shock or detonation wave. It can be a useful phenomenon for rendering safe an explosive charge or an unwanted process that hinders the intended detonation of a charge. Both corner turning and shock desensitization are highly time dependent, and thus must be numerically modeled by reactive flow models that account for variable energy release rates in various regions of the flow field.

Corner turning is not a major concern for most solid explosives that are more shock sensitive than TATB. Detonation waves in these explosives easily turn 90˚ corners with no time delay and no unreacted explosive left behind. PBX formulations based on insensitive high explosives like TATB leave regions of unreacted and/or partially reacted material (often called dead zones) when their detonation waves attempt to turn 90˚ corners without confinement. When confining material is present in the corner, TATB detonation waves propagate around the corner with no time delays and no dead zones. The first experimental and hydrodynamic modeling studies were done at the Phermex X-ray machine at Los Alamos National Laboratory and reported by Mader.[2,3] Further quantitative experimental data on the sizes of the dead zones left by TATB PBX's were reported by Cox and Campbell.[4] An acceptance test for the diverging TATB PBX detonation waves in various batches of TATB at various initial densities was developed for insensitive high explosives at the Pantex plant. The Pantex corner turning test was discussed and numerically modeled by Tarver.[5] This test measures the breakout time and distance along a cylindrical charge initiated by a smaller diameter HMX cylinder, so corners are not actually turned, but dead zones are observed. Recently a corner turning test using X-ray radiographs and time of arrival pins called the Hockey Puck test was developed at Lawrence Livermore National Laboratory.[6] Both LX-17 (92.5% by weight TATB and 7.5% KelF binder pressed to 1.905 g/cm^3 or 98% theoretical maximum density) and PBX 9502 (95% TATB and 5% KelF pressed to 1.895 g/cm3 or 97.5% theoretical maximum density) were studied. The measured dead zones and times of arrival for both PBX's were accurately calculated by the Ignition and Growth reactive flow model.[6,7]

The most detailed experiments of TATB corner turning and dead zone formation are those done using proton radiography at Los Alamos National Laboratory.[8,9] The greater penetrating power of high

energy protons compared to X-rays allows finer structures of the dead zones to be observed. The proton radiography experiments showed that the dead zones formed by PBX 9502 traversing 90° corners lasted for several microseconds longer than previously observed. The original Ignition and Growth reactive flow model creates the correct size and shape of the observed dead zones, but does allow them to react at relatively long times after the detonation wave has passed. DeOliveira et al.[10] added an additional term to the Ignition and Growth model that allows for time dependent shock desensitization of a compressed region of explosive and no subsequent reaction in that region. This modification allows the Ignition and Growth LX-17 and PBX 9502 detonation model parameters to accurately simulate all of the observed time of arrival and dead zone effects.

In this paper, five experiments are reported in which the ability of LX-17 detonation waves to turn two corners of an embedded steel disc is tested. Preliminary LX-17 Ignition and Growth modeling showed that dead zones formed near both corners of the steel discs, but that the LX-17 detonation waves continued to propagate around both corners. The five experiments were then designed based on those modeling predictions.

The second objective of these five experiments is to determine some of the shock desensitization properties of LX-17. Shock desensitization is a well-known phenomenon in solid explosives. In the original study, Campbell and Travis[11] impacted large PBX 9404 (94% HMX, 3% nitrocellulose, and 3% chloroethylphosphate) and Composition B (RDX/TNT) charge with weak shocks on one edge and initiated detonation on another edge. They then measured the interactions of these detonation waves with weak shocks of various strengths. For a certain shock pressure region (1 – 2.4 GPa) in both PBX 9404 and Composition B, the detonation waves propagated a few millimeters into the pre-compressed explosive and then failed abruptly. The measured time duration before failure was close to the experimental measured shock initiation time for that specific shock pressure. For shock pressures below 1 GPa, which did not pre-compress the unreacted explosive to maximum its density, the detonation waves wavered slightly but continued to detonate through the pre-compressed explosive that still contained hot spot reaction sites. At shock pressures greater than 2.4 GPa, the detonation waves encountered compressed explosives with growing hot spots so they continued to detonate through the compressed, reacting explosives.

Along with these original experiments, many shock desensitization studies have been done using various explosives using weak shocks plus detonation waves, two shocks, or reflected shocks.[12-18] Only two studies of TATB-based PBX's have been published. Tarver et al.[19] impacted LX-17 cylindrical charges containing embedded manganin pressure gauges backed by aluminum, copper, or tantulam discs at various input pressures and observed shock desensitization behind the first shock at certain pressures. However, to obtain measurable growth of reaction in LX-17 a sustained shock pressure of about 7 – 8 GPa is required. Since reflection only approximately doubles the shock pressure, these experiments did not study initial shock pressures below 4.4 GPa. Shock desensitization was observed, and the experiments were calculated with the Ignition and Growth model using a range of compressions under which LX-17 would not ignite.[19] Excellent agreement with pressure growth or no growth (shock desensitization) was obtained for both the initial and reflected shocks. Mulford et al.[20] used line detonators in large EDC35 (95% TATB/5% KelF) charges to create weak shocks that interacted with detonation waves at various angles. They estimated that the weak shock pressures were about 1.5 GPa and that shock desensitization occurred in about 0.2 μs or within 1 - 2 mm of propagation after the interactions. Mulford et al. observed shock desensitization of EDC35 with both normal and parallel interactions of the detonation waves with the weak shocks.

The five experiments presented in the next section were designed to pre-compress LX-17 in the 1 – 2 GPa pressure range by diverging shocks propagating through the steel shadow plates as the corner turning LX-17 detonation waves are propagating. The LX-17 detonation waves then arrive in weakly shocked regions of pre-compressed LX-17. If the weak shock pressures are high enough and are applied long enough, the pre-shocked LX-17 becomes shock desensitized and the detonation waves fail. If the shocks are not strong enough or too strong, the detonation waves continue to detonate. The Ignition and Growth model with desensitization predicted that shock desensitization would occur in all five experiments based on input parameters estimated from higher pressure, Hockey Puck dead zone experiments.[10]

EXPERIMENTS

Five experiments are discussed which investigated both detonation wave corner turning and shock desensitization of LX-17. Figure 1 contains a colored graphic cross section of one of the double

corner turning and shock desensitization experiments. The small white region inside the interior gray region is the LX-16 used to initiate detonation, and this gray region is the 303 stainless steel shadow plate. The bright yellow region is the UF TATB hemispherical booster, which is fine particle TATB pressed to 1.80 g/cm^3 or 93% theoretical maximum density (TMD). The yellow/red region is the main LX-17 charge. The top and bottom gray regions are the aluminum witness plates. The bottom aluminum plate contains three time-of-arrival pins to check that a diverging LX-17 detonation was fully initiated.

Upon firing, small PETN based LX-16 explosive charges initiated hemispherical UF TATB boosters, which in turn initiated LX-17 hemispherical detonations. The LX-17 detonations propagated outward until they reached the aluminum plates, which were instrumented with photonic Doppler velocimetry (PDV) probes[21] to measure the free surface velocity histories of the top aluminum plates. X-ray radiographs and framing camera images were taken at various times. The LX-17 detonations propagated around the two corners of the steel shadow plates and into thin LX-17 regions between the steel shadow plates and the top aluminum plates. The detonation waves were met in these regions by weak diverging shock waves that had propagated through the steel shadow plates and imparted 1 to 2 GPa pressures to the unreacted LX-17 above them. These shock pressures compressed and shock desensitized LX-17, resulting in failures of LX-17 detonation waves when they reached the pre-shocked LX-17.

Figures 2 – 6 contain the schematic cross sections of the five experiments labeled E3 – E7 with the dimensions in millimeters. As shown in Fig. 2 for experiment E3, the UF TATB booster has a radius of 19 mm and is attached to the bottom of the 303 stainless steel shadow plate, which is 10 mm thick and has a 21.5 mm radius. The LX-17 cylindrical charge is 60 mm radius by 76 mm long, weighing 1.6 kilograms. The top and bottom aluminum 6061-T6 plates are 6 mm thick. The LX-17 between the top aluminum plate and the stainless steel disc is 10 mm thick. The PDV probes are placed at 0, 10, 20, 25, 30, 35, 40, and 50 mm from the centerline on the free surface of the top aluminum plate. Three time-of-arrival pins are placed at the interface of the LX-17 charge and the bottom aluminum plate on the centerline and 30 mm to either side of center to measure the average propagation of the diverging detonation wave through the UF TATB and LX-17. Not shown is the small disc of LX-16 that is detonated above the center of the UF TATB booster. Figure 3 shows the dimensions of experiment E4, which are

the same as those for E3, except that the LX-17 between the steel shadow plate and the top aluminum plate is 20 mm thick. This increased LX-17 thickness was used to determine whether a larger thickness of LX-17 would be completely shock desensitized by the decaying weak shock wave emerging from the steel shadow plate. Figure 4 shows the dimensions of experiment E5 in which the stainless steel shadow plate has a radius of 43 mm and the LX-17 charge has a radius of 80 mm. The stainless steel shadow plate and the LX-17 between the steel and the top aluminum plate are both 10 mm thick. This larger radius steel shadow plate was used to determine whether a longer LX-17 detonation run distance along a steel plate would change the corner turning and shock desensitization properties. The PDV probes were placed at 0, 20, 30, 35, 45, 55, 65, and 75 mm from the centerline. Figure 5 illustrates that experiment E6 is identical to E5 except that the LX-17 between the steel shadow plate and the top aluminum plate is 20 mm thick instead of 10 mm. The fifth experiment E7, shown in Fig. 6, employed a more complex shaped steel shadow plate that resembled a "gull wing" or a "pith helmet." In this experiment, the LX-17 detonation wave has only one sharp point to propagate around after 24 mm of propagation. It then travels as a converging wave into 30 mm of pre-compressed LX-17 that narrows to 10 mm at the centerline. This steel shadow plate design was used to determine whether or not the LX-17 in this more complex geometry is desensitized by the weak shock wave emerging from the steel shadow plate. If not, the converging LX-17 detonation wave can overcome the shock desensitization effect and continue to propagate.

Both the PDV measured free surface velocity histories and X-rays taken at times after the LX-17 detonation waves reached the centerlines of the LX-17 charges between the top aluminum plates and the steel shadow plates are used to show whether shock desensitization has caused failure of the LX-17 detonation wave in each geometry. Early time X-rays and the PDV free surface velocity histories taken at radii greater than those of the steel shadow plates show whether the LX-17 successfully turned both steel corners in experiments E3 – E6 and the one edge in experiment E7. Calculated head-on, angled, or sideways collisions of LX-17 detonations with 6 mm thick aluminum discs produced free surface jump-off velocities of over 2 km/s. A failed detonation wave produced a much lower free surface jump-off velocity, because its shock front pressure is much less than that of a self-sustaining detonation wave. The later time aluminum free surface histories are also very different from those produced by detonation.

Before the experiments were fired, there was uncertainty about an LX-17 detonation wave's ability to turn the second corner of the steel shadow plate. It is well known that the turning of the first corner leaves a "dead zone" of unreacted or partially reacted TATB. Such a "dead zone" could cause a perturbed detonation wave to fail when it reaches the second corner after only 1 cm of propagation along the side of the plate. There was also uncertainty about the weak shock that propagates through the steel shadow plate and into unreacted LX-17 being strong enough to compress the LX-17 to full density and shock desensitize it.

The experimental results clearly showed that the divergent LX-17 detonation wave turned both corners of the steel shadow plate and that the shock desensitization of the LX-17 between the steel shadow and the top aluminum plate was sufficient to "kill" the LX-17 detonation wave in all five experiments. Figures 7 – 11 show the X-ray radiographs taken 30 μs after the electrical circuits were fired for experiments 3 – 7, respectively. Since the detonator function time was 2 μs, these X-rays show the hydrodynamic flow at 28 μs after the LX-16 initiated. This time is longer than the times required for the LX-17 detonation waves to propagate around the steel plates and through the desensitized explosives to reach the axes of all five experiments. The lighter regions in Figs. 7 – 11 are the expanding LX-17 detonation products, while the darker regions between the steel and aluminum plates are the denser shock desensitized unreacted (or partially reacted) LX-17. The shapes of the top aluminum witness plates clearly demonstrate that they were accelerated much faster by the LX-17 detonation waves at radii greater than the radii of the steel plates than by the inert shocks in the regions directly above the steel plates. The interfaces between lighter detonation products and darker desensitized LX-17 imply that the LX-17 detonation waves propagated only a few millimeters into the pre-shocked LX-17 before failing to detonate. This is consistent with the two shock desensitization experimental studies on TATB based explosives[19,20] and with the Ignition and Growth reactive flow modeling predictions discussed in the following section.

IGNITION AND GROWTH MODEL

The Ignition and Growth reactive flow model of shock initiation and detonation has been used to understand for many shock initiation and detonation studies of solid explosives and propellants in several 1D, 2D, and 3D codes.[22,23] The set of Ignition and Growth parameters for detonating LX-17 is well

established by modeling many 1D, 2D and some 3D experiments.[24] The model uses two Jones-Wilkins-Lee (JWL) equations of state, one for the unreacted explosive and one for its reaction products, in the temperature dependent form:

$$p = Ae^{-R1V} + Be^{-R2V} + \omega C_v T/V \qquad (1)$$

where p is pressure in megabars, V is relative volume, T is temperature, ω is the usual Gruneisen coefficient, C_V is the average heat capacity, and A, B, R_1, and R_2 are constants. The reaction rate law for the conversion of explosive to products is:

$$dF/dt = \underset{0<F<F_{igmax}}{I(1-F)^b(\rho/\rho_o - 1 - a)^x} + \underset{0<F<F_{G1max}}{G_1(1-F)^cF^dp^y} + \underset{F_{G2min}<F<1}{G_2(1-F)^eF^gp^z} \qquad (2)$$

where F is the fraction reacted, t is time, ρ is the current density, ρ_o is the initial density, and I, G_1, G_2, a, b, c, d, e, g, x, y, and z are constants. The mixture equations assume pressure and temperature equilibration between the unreacted explosive and its reaction products.

The unreacted JWL for LX-17 is fit to experimental shock compression data and nanosecond time resolved von Neumann spike data for detonating LX-17.[25] The reaction product JWL equation of state is fit to the wall velocity expansion data from cylinder tests and laser interferometric plate push data for steady[26,27] and overdriven detonations.[28] The three-term rate law describes the three stages of reaction generally observed in shock initiation and detonation of heterogeneous solid explosives. For solid explosive detonation modeling, the first term of Equation (2) represents the ignition of the explosive as it is compressed by the leading 3D shock wave creating hot regions at the triple shock interactions.[29] The fraction of explosive ignited is assumed to be equal to the void volume of the pressed explosive and is reacted in less than a nanosecond. For LX-17 at 1.905 g/cm^3, the initial void volume is 2%. The second reaction rate in Eq. (4) models the rapid formation of the major reaction product gases (CO_2, N_2, H_2O, CO, etc.) in highly vibrationally excited states and their subsequent expansion and equilibration.[29] This process for LX-17 has been measured to take approximately 80 nanoseconds by several techniques.[30,31] The third term in Eq. (4) is used to describe the relatively slow diffusion controlled formation of nanometer size solid carbon particles (diamond, graphite, or amorphous carbon) from single or small groups of carbon atoms. For LX-17, the last 20% of the chemical energy release is assumed to be due to solid

graphite nanoparticle formation in a diffusion controlled process. Experimentally, the carbon formation in LX-17 has been observed to take approximately 300 nanoseconds.[32] The overall reaction zone length for detonating LX-17 is therefore approximately 3 mm or 400 nanoseconds.

Table 1 lists the equation of state and reaction rate parameters used in the Ignition and Growth UF TATB and LX-17 detonation model. The UF TATB reactive flow model must be used, because UF TATB also exhibits a finite thickness reaction zone and measurable wave curvature. The detailed shape and strength of the UF TATB detonation wave influences the subsequent detonation wave structure in the LX-17.[6] The LX-17 parameters were determined by matching nanosecond time resolved data from several 1D and 2D detonation experiments,[24] and have been applied to several other experiments.[33,34] Also listed in Table 1 are the Chapman-Jouguet (C-J) and JWL reaction product parameters for the instantaneous detonation of LX-16 and the Gruneisen equation of state parameters for the steel and aluminum plates.

As discussed in the Introduction, to model shock desensitization in doubly shocked LX-17, a second compression constant was added to the first term of the reaction rate law in Eq. (2) by Tarver et al.[19] That allowed that the reaction rate to be set equal to zero when the LX-17 was shocked within a certain range of compressions. This assumption worked well for LX-17 shock desensitization in reflected shock experiments. However, for several other explosives, it has been shown that shock desensitization is time dependent. The failure of detonation in the pre-compressed explosive requires times approximately equal to the times for shock initiation at various shock pressures.[11] For TATB PBX's, it has also been shown using proton radiography on corner turning experiments that dead zones can exist for relatively long times after detonation waves turn corners.[8,9] The regular Ignition and Growth model creates dead zones and propagates around one corner extremely accurately, but does eventually allow the partially reacted dead zone regions to react at late times. Thus, to model longer lasting dead zones, a time dependent desensitization rate law was added to the Ignition rate term in Eq. (2) by DeOliveira et al.[10] The desensitization rate S is defined as:

$$S = Ap(1 - \phi)(\phi + \varepsilon) \tag{3}$$

where A is a constant, p is the shock pressure, ε is a small constant, and ϕ varies from zero in a pristine explosive to one in a fully desensitized explosive. The density threshold a in Eq. (2) is redefined to be a linear function of ϕ:

$$a(\phi) = a_0(1-\phi) + a_1(\phi) \tag{4}$$

where a_0 and a_1 are constants. The relative density threshold for ignition of the pristine explosive becomes 1 + a_0, and, for the fully desensitized explosive, the relative density for ignition becomes 1 + a_1. Additionally, the second reaction rate term in Eq. (2) is modified so that it turns on only when F exceeds a minimum F_{G1min}, which is a linear function of ϕ:

$$F_{G1min}(\phi) = F_c\phi \tag{5}$$

where F_c is a constant related to the initial porosity. This second modification provides a competition between desensitization and reaction growth and thus determines an extinction mechanism. This modification introduces four new parameters: A, ε, a_1, and F_c. Unfortunately, no well-defined, time resolved experiments, such as those of Campbell and Travis,[11] have yet been done on LX-17. DeOliveria et al.[10] derived reasonable values of A = 1000, ε = 0.001, a_1 = 0.50, and Fc = 0.01 to produce reasonable dead zones for the hockey puck corner turning experiments. For lower pressures, these values yield desensitization times of 1.29 μs for a 1 GPa shock and 0.26 μs for a 5 GPa shock. Mulford et al.[20] estimated a time of 0.2 μs for shock desensitization of PBX 9502 subjected to a 1.5 GPa shock pressure. The distances at which the LX-17 detonation waves failed in the pre-shocked regions shown in Figs. 7 – 11 ranged from 5 to 8 mm, which are consistent with desensitization times of approximately 1 μs, based on LX-17's detonation velocity of 7.63 mm/μs.

Several snapshots of the Ignition and Growth model calculations for experiment E3 show the details of the LX-17 detonation wave corner turning and the shock desensitization of the LX-17 between the steel and aluminum plates. Figure 12 shows the fraction reacted contours in the detonating LX-17 at 8 μs after electrical firing (6 μs of detonation flow) that illustrates the diverging detonation wave, the turning of the first steel corner, and the beginning of the formation of the first "dead zone". In Fig. 12 the "a" contour denotes complete reaction (F=1), the "b" contour denotes 80% reaction, and the "c" – "i" contours denote 70, 60, … 10% reaction. The calculational geometry is inverted from that shown in Fig.

1, and only half of the symmetrical problem is shown in Fig. 12. Figure 13 shows similar fraction reaction contours at 9 μs after electrical firing (7 μs of detonation flow) in a small region near the steel plate. The calculated "dead zone" at the first corner of the steel plate is evident, as are two other areas of partial reaction beyond the second corner of the plate. The LX-17 detonation wave, although it is perturbed by the steel plate, continues to propagate outward and enters the pre-compressed LX-17 layer just before this 9 μs snapshot. The LX-17 detonation wave first interacts with the aluminum plate at a distance of about 10 mm greater than the radius of the steel plate. Figure 14 shows the calculated pressure contours in the pre-compressed LX-17 layer at 8.5 μs, which is just before the LX-17 detonation wave arrives at its outer boundary. The maximum pressure in Fig. 14 is 2.14 GPa, and much of the LX-17 has compressed by the rightward moving shock to between 1.07 GPa (contour "e") and 1.29 GPa (contour "f"). Figure 15 shows the pressure contours in the shock desensitized LX-17 region at 10.5 μs behind the leftward moving, failed detonation wave that has traveled approximately half way through the desensitized region. The maximum pressure is 21.8 GPa at the aluminum plate boundary. The main shock front has a pressure of approximately 11 GPa (contour "e" in Fig. 15). Figure 16 shows the calculated pressures in the desensitized LX-17 region at 14.5 μs, which is after reflection at the centerline so the shock front is moving to the right in Fig. 16. The maximum pressure is 7 GPa, and most of the desensitized LX-17 near the reflected shock is between 3.4 GPa (contour "e") and 5.6 GPa (contour "h"). The shape of the bottom boundary of the desensitized region shows how the aluminum plate is being accelerated by the multiply shocked desensitized LX-17.

COMPARISONS OF EXPERIMENTAL AND CALCULATED RESULTS

The main comparisons between the experimental and calculated shock desensitization results are the jump-off times for the top aluminum plates and the subsequent free surface velocity histories measured by the PDV probes. The measured PDV free surface velocity histories are shown in Figs. 17 – 21 for experiments E3 – E7, respectively, while the corresponding Ignition and Growth desensitization model calculated free surface velocity histories are shown in Figs. 22 – 26. Two microseconds were added to the calculated times to account for the measured detonator function times. Both the experiments and calculations show that the LX-17 at larger radii than the steel shadow plate radii clearly detonated and produced jump-off velocities greater than 2 km/s. Since the LX-17 detonation waves were

curved by turning two corners, they impacted the top aluminum plates at various angles and at various times, thus producing different measured initial jump-off velocities in the 2 – 2.4 km/s range. The calculated initial jump-off velocities varied from 2 – 2.5 km/s, and, in general, agreed well with the individual experimental measurements. For example, experiments E5 and E6 showed lower initial jump-off velocities near 2.1 – 2.2 km/s in both the calculations and experiments, while experiments E4 and E7 yielded higher jump-off velocities near 2.4 – 2.5 km/s in both. The interaction of the LX-17 detonation waves with the aluminum plates at low angles produced the lower calculated jump-off velocities for experiments E5 and E6, while higher angle interactions produced higher jump-off velocities for experiments E3, E4 and E7. The calculated jump-off velocities for experiment E3 were higher than measured. The calculated jump-off times for these outer PDV probes agreed well with the experimental measurements for all five experiments. This implies that the calculated LX-17 detonation wave propagations accurately simulate the entire reactive flow processes in all five experiments. The experimental and calculated subsequent aluminum free surface velocity histories agree and are typical of relatively thin plates accelerated by detonation waves arriving at various angles.[24,27,34]

The measured free surface velocity histories at radii less than or slightly greater than those of the steel shadow plates show much lower initial jump-off velocities and more complex acceleration histories caused by the arrival of various shocks and their subsequent reflections in the shock desensitized LX-17 region. Most of these free surface probes eventually reach approximately 1.5 km/s after several shock compressions over 10 – 12 μs. These velocity histories along with the X-ray radiographs in Figs. 7 – 11 clearly show that these regions of the aluminum plates are not being driven by LX-17 detonation waves. Similar calculated velocity histories for all five experiments imply that the entire regions of LX-17 between the steel shadow plates and the aluminum witness plates were totally desensitized by the weak shock waves [ϕ = 1 in Eq. (3)]. Little or no chemical energy was released in these LX-17 regions. The calculated arrival times and magnitudes of the free surface velocity increases produced by the inert shock waves and their reflections reproduce the measurements quite well for all five experiments. Particularly encouraging was the agreement between the measured and calculated arrival times and magnitudes of the free surface velocity jumps caused by the failed detonation wave arriving at the charge axis at approximately 20 μs in experiments E5 and E6 shown in Figs. 12, 13, 19, and 20. Some of the calculated

aluminum free surface velocities at very small radii in experiments E4, E6, and E7, which contain 20 mm thick desensitized LX-17 layers, are lower than measured at early times. This could mean that some LX-17 was not completely desensitized ($\phi < 1$) when the failing detonation wave arrived and thus partially reacted. This can be checked by rerunning the Ignition and Growth calculations with a slower desensitization rate S in Eq. (3) that does not allow ϕ to reach one. Actually, measurements of LX-17 desensitization rates in head-on shock and detonation wave interaction experiments, such as those of Campbell and Travis,[11] are required to further quantify the time dependent shock desensitization process in LX-17.

CONCLUSIONS

The five experiments discussed in this paper clearly demonstrated for the first time the ability of a LX-17 detonation wave to successfully turn the two corners of a steel shadow plate. The Ignition and Growth reactive model for detonating LX-17 predicted the double corner turning with good timing accuracy. Since detonation waves are often asked to propagate through abrupt or gradual geometric changes, accurate reactive models are needed to design explosive charges containing such changes. X-ray radiographs, framing camera images, and time resolved PDV probe measurements of the free surfaces of aluminum witness plates clearly demonstrated that LX-17 between the steel and aluminum plates was pre-compressed by a weak divergent shock wave and left shock desensitized by the time the LX-17 detonation waves arrived in all five experiments. Jump-off times and PDV aluminum free surface velocity histories at positions less than the radii of the steel shadow plates calculated using the desensitization rate term in the Ignition and Growth reactive flow model for LX-17 agreed well with the experimental PDV measurements for all five experiments. This model can thus be used for predicting shock desensitization of LX-17 with confidence. To improve the understanding of the time dependence of LX-17 over the relevant range of shock pressures, well controlled head on interaction experiments, similar to those done by Campbell and Travis,[11] need to be done. The desensitization rate in the Ignition and Growth model would then be calibrated to this data and yield predictions with increased confidence. The more physically based Statistical Hot Spot reactive flow model[35] has been demonstrated to predict shock desensitization, but requires more fundamental experimental and theoretical knowledge of hot spot

formation, growth, death, and coalescence processes to allow its complete normalization for a particular explosive.

Shock desensitization has long been an interesting but under studied process due to its transient nature. Obtaining a more thorough understanding of this process through combined experimental and modeling efforts may lead to practical uses of weak shock waves that desensitize and thus render safe large explosive charges. Conversely, unwanted shock desensitization of regions of large explosive charges may be avoided.

ACKNOWLEDGMENTS

The author thanks: Mark Hart, who envisioned, designed and analyzed these experiments; Ted Strand who made the PDV velocimetry measurements; the bunker crew who fired the experiments; and David Hare, who did many preliminary reactive flow calculations. This work was performed under the auspices of the United States Department of Energy by the Lawrence Livermore National Laboratory under Contract No. DE-AC52-07NA2734.

TABLE 1. MODELING PARAMETERS FOR LX-17, UF TATB, LX-16, ALUMINUM AND STEEL

A. LX-17	ρ_o =1.905 g/cm^3		
UNREACTED JWL	PRODUCT JWL	REACTION RATES	
A=77810 GPa	A=14.81.05 GPa	I=4.0x10^6 μs^{-1}	
B= -5.031 GPa	B=63.79 GPa	a=0.22	
R_1=11.3	R_1=6.2	b=0.667	
R_2=1.13	R_2=2.2	x=7.0	F_{igmax}=0.02

ω=0.8938	ω=0.5	G_1=0.0045 GPa$^{-3}\mu s^{-1}$
C_V=2.487x10^{-3} GPa/K	C_V=1.0x10^{-3} GPa/K	c=0.667
T_o = 298$^{\bullet}$K	E_o=6.9GPar	d=1.0
Shear Modulus=3.54 GPa		y=2.0 F_{G1max}=0.8
Yield Strength=0.2 GPa		G_2=0.30 GPa$^{-1}\mu s^{-1}$
		e=0.667 z=1.0
		g=0.667 FG2min=0.8
B. Ultrafine TATB	ρ_o =1.80 g/cm^3	
UNREACTED JWL	PRODUCT JWL	REACTION RATES
A=63207 GPa	A=1205.026 GPa	I=4.0x10$^6\mu s^{-1}$
B= -4.472 GPa	B=60.2513 GPa	a=0.214
R_1=11.3	R_1=6.2	b=0.667
R_2=1.13	R_2=2.2	x=7.0 F_{igmax}=0.071
ω=0.8938	ω=0.5	G_1=0.22 GPa$^{-2}\mu s^{-1}$
C_V=2.487x10^{-3} GPa/K	C_V=1.0x10^{-5} GPa/K	c=0.667
T_o = 298$^{\bullet}$K	E_o=6.9 GPa	d=1.0
Shear Modulus=3.0 GPa		y=2.0 F_{G1max}=1.0
Yield Strength=0.2 GPa		G_2=0.6 GPa$^{-1}\mu s^{-1}$
		e=0.667 z=1.0
		g=0.667 F_{G2min}=0.8

C. GRUNEISEN EQUATION OF STATE PARAMETERS FOR ALUMINUM AND STEEL

$$P = \rho_o c^2 \mu[1+(1-\gamma_o/2)\mu - a/2\mu^2]/[1-(S_1-1)\mu - S_2\mu^2/(\mu+1) - S_3\mu^3/(\mu+1)^2]^2 + (\gamma_o + a\mu)E,$$

where $\mu = (\rho/\rho_o - 1)$ and E is thermal energy

INERT	ρ_o(g/cm^3)	c(mm/μs)	S_1	S_2	S_3	γ_o	a
Al 6061	2.703	5.24	1.4	0.0	0.0	1.97	0.48
Steel	7.90	4.57	1.49	0.0	0.0	1.93	0.5

D. JONES – WILKINS – LEE (JWL) PARAMETERS FOR LX-16 C-J DETONATION

LX-16 (96% PETN, 4% FPC 461) ρ_o = 1.7g/cm^3; D = 0.7963 cm/μs; P_{CJ} = 30.507 GPa;
A = 516.784 GPa; B = 24.491 GPa; R_1 = 4.5; R_2 = 1.5; ω = 0.29; Eo = 9.86 GPa-cc/cc-g

REFERENCES

1. F. P. Bowden and Y. D. Yoffe, Initiation and Growth of Explosion in Liquids and Solids, Cambridge Science Classics, University Press, Cambridge, 1985.

2. C. L. Mader, Sixth Symposium (International) on Detonation, Naval Surface Weapons Center ACR-221, Coronado, CA, 1976, p. 405.

3. C. L. Mader, Numerical Modeling of Detonation, University of California Press, Berkeley, 1979.

4. M. Cox and A. W. Campbell, Seventh Symposium (International) on Detonation, Naval Surface Warfare Center NSWC MP82-334, Annapolis, MD, 1981, p. 624.

5. C. M. Tarver, Propellants, Explosives, Pyrotechnics **15**, 132 (1990).

6. C. M. Tarver, Propellants, Explosives, Pyrotechnics **30**, 109 (2005).

7. M. L. Garcia and C. M. Tarver, Thirteenth International Detonation Symposium, Office of Naval Research ONR 351-07-2, Norfolk, VA, 2006, p. 63.

8. E. N. Ferm, C. L. Morris, J. P. Quintana, P. Pazuchanic, H. Stacy, J. D. Zumbro, G. Hogan, and N. King, Shock Compression of Condensed Matter-2001, AIP Conference 620, Atlanta, GA, 2002, p. 966.

9. C. L. Mader, J. D. Zumbro, E. N. Ferm, M. Gittings, and R. Weaver, Twelfth International Detonation Symposium, Office of Naval Research ONR-333-05-2, San Diego, CA, 2002, p. 55.

10. G. de Oliveira, A.K. Kapila, W, Schwendeman, J. B. Bdzil, W. D. Henshaw, and C. M. Tarver, Thirteenth International Detonation Symposium, Office of Naval Research ONR 351-07-2, Norfolk, VA, 2006, p. 13.

11. A. W. Campbell and J. R. Travis, Eighth Symposium (International) on Detonation, Office of Naval Research NSWC MP86-194, Albuquerque, NM, 1985, p. 1057.

12. M. C. Chick and D. J. Hatt, Seventh Symposium (International) on Detonation, Naval Surface Warfare Center NSWC MP82-334, Annapolis, MD, 1981, p. 352.

13. A. W. Campbell, W. C. Davis, J. B. Ramsay, and J. R. Travis, Phys. Fluids **4**, 511 (1961).

15. D. W. Woodhead, Nature **183**, 1756 (1979).

16. V. M. Boyle and D. L. Pilarsky, Seventh Symposium (International) on Detonation, Naval Surface Warfare Center NSWC MP82-334, Annapolis, MD, 1981, p. 906.

17. Y. V. Bat'kov, B. L. Glushak, and S. A. Novikov, Combustion, Explosion, and Shock Waves **31**, 482 (1995).

18. S. A. Bordzilovskii and S. M. Karakhanov, Combustion, Explosion, and Shock Waves **31**, 227 (1995).

19. C. M. Tarver, T. M. Cook, P. A. Urtiew, and W. C. Tao, Tenth Symposium (International) on Detonation, Office of Naval Research ONR 33395-12, Boston, MA, 1993, p. 696.

20. R. N. Mulford, D. C. Swift, A. M. Collyer, and S. J. White, Proc. 5th Symposium on High Dynamic Pressures, St. Malo, France, 1, 81 (2003).

21. O. T. Strand, D. R. Goosman, C. Martinez, T. L. Whitworth, and W. W. Kuhlow, Rev. Sci. Instrum. **77**, 083108 (2006).

22. C. M. Tarver, J. O. Hallquist, and L. M. Erickson, Eighth Symposium (International) on Detonation, Naval Surface Weapons Center NSWC MP86-194, Albuquerque, NM, 1985, p. 951.

23. K. Bahl, G. Bloom, L. Erickson, R. Lee, C. Tarver, W. Von Holle, and R. Weingart, Eighth Symposium (International) on Detonation, Naval Surface Weapons Center NSWC MP86-194, Albuquerque, NM, 1985, p. 1045.

24. C. M. Tarver and E. M. McGuire, Twelfth International Detonation Symposium, Office of Naval Research ONR-333-05-2, San Diego, CA, 2002, p. 641.

25. B. Hayes and C. M. Tarver, Seventh Symposium (International) on Detonation, Naval Surface Warfare Center NSWC MP82-334, Annapolis, MD, 1981, p. 1029.

26. C. M. Tarver, J. W. Kury, and R. D. Breithaupt, J. Applied Physics **82**, 3771 (1997).

27. C. M. Tarver, W. C. Tao, and C. G. Lee, Propellants, Explosives, Pyrotechnics, **21**, 238 (1996).

28. L. G. Green, C. M. Tarver, and D. L. Erskine, Ninth Symposium (International) on Detonation, Office of the Chief of Naval Research, OCNR 113291-7, Portland, OR, 1989, p. 670.

29. C. M. Tarver, J. Phys. Chem. A **101**, 4845 (1997).

30. S. A. Sheffield, D. D. Bloomquist, and C. M. Tarver, J. Chem. Phys. **80,** 3831 (1984).

31. C. M. Tarver, N. L. Parker, H. G. Palmer, B. Hayes, and L. M. Erickson, J. Energetic Materials **1**, 213 (1983).

32. W. L. Seitz, H. L. Stacy, R. Engelke, P. K. Tang, and J. Wackerle, Ninth Symposium (International) on Detonation, Office of the Chief of Naval Research, OCNR 113291-7, Portland, OR, 1989, p. 657.

33. C. M. Tarver, Shock Compression of Condensed Matter – 2005, AIP Conference Proc. 845, Baltimore, MD, 2006, p. 1026.

34. C. M. Tarver and S. K. Chidester, Shock Compression of Condensed Matter – 2007, AIP Conference Proc. 955, Waikoloa, Hawaii, 2007, p. 429.

35. A. L. Nichols III and C. M. Tarver, Twelfth International Detonation Symposium, Office of Naval Research ONR-333-05-2, San Diego, Ca, 2002, p. 489.

FIGURE CAPTIONS

Figure 1. Graphic cross section of a double corner turning and shock desensitization experiment

Figure 2. Schematic cross section of experiment E3 (dimensions in mm)

Figure 3. Schematic cross section of experiment E4 (dimensions in mm)

Figure 4. Schematic cross section of experiment E5 (dimensions in mm)

Figure 5. Schematic cross section of experiment E6 (dimensions in mm)

Figure 6. Schematic cross section of experiment E7 (dimensions in mm)

Figure 7. X-ray of experiment E3 taken at 30 microseconds

Figure 8. X-ray of experiment E4 taken at 30 microseconds

Figure 9. X-ray of experiment E5 taken at 30 microseconds

Figure 10. X-ray of experiment E6 taken at 30 microseconds

Figure 11. X-ray of experiment E7 taken at 30 microseconds

Figure 12. Fraction reacted contours calculated for experiment E3 at 8 μs

Figure 13. Fraction reacted contours calculated for experiment E3 at 9 μs

Figure 14. Calculated pressure contours in desensitized LX-17 for experiment E3 at 8.5 μs

Figure 15. Calculated pressure contours in desensitized LX-17 for experiment E3 at 10.5 μs

Figure 16. Calculated pressure contours in desensitized LX-17 for experiment E3 at 14.5 μs

Figure 17. PDV aluminum free surface velocity histories measured in experiment E3

Figure 18. PDV aluminum free surface velocity histories measured in experiment E4

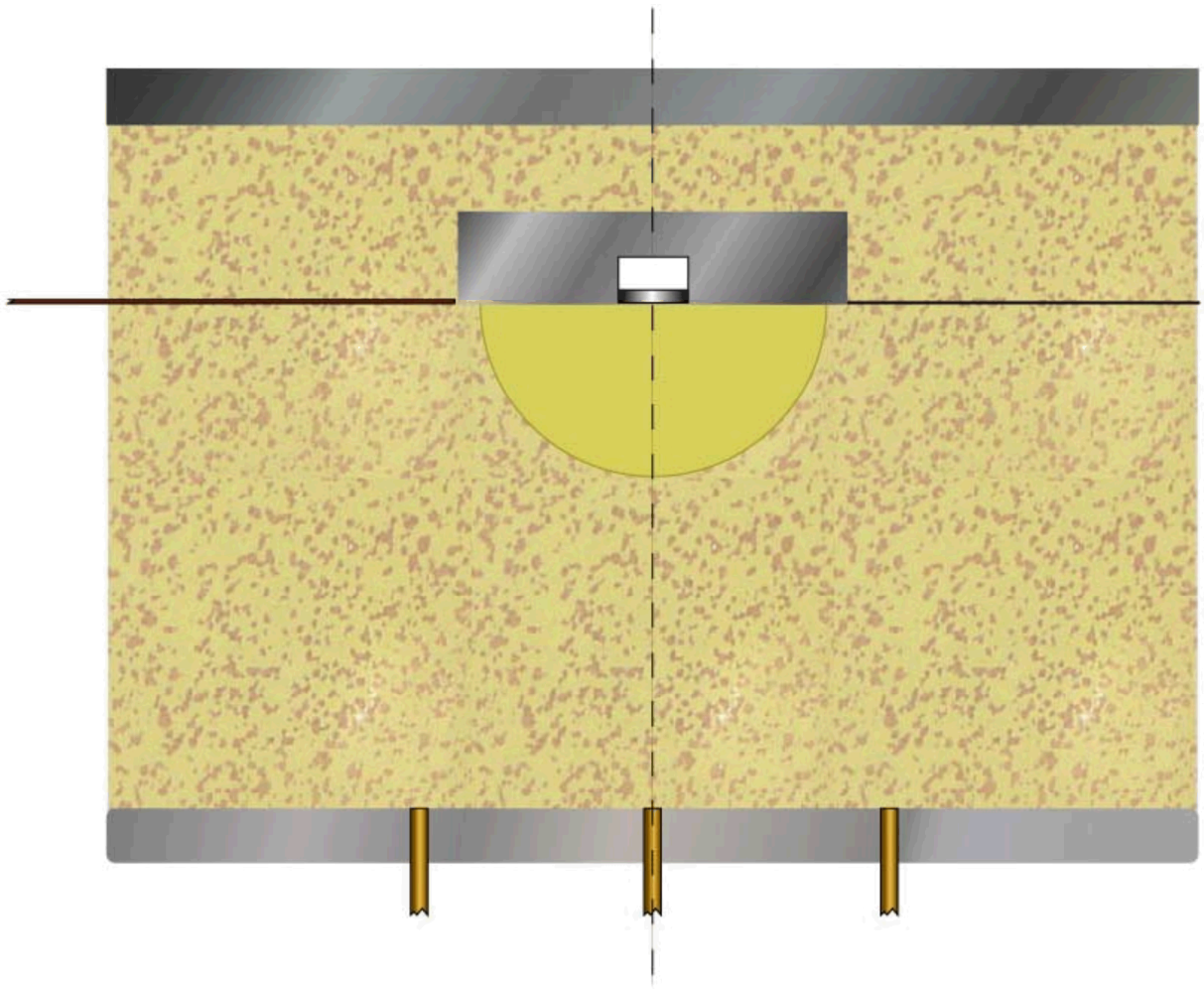

Figure 1. Graphic cross section of a double corner turning and shock desensitization experiment

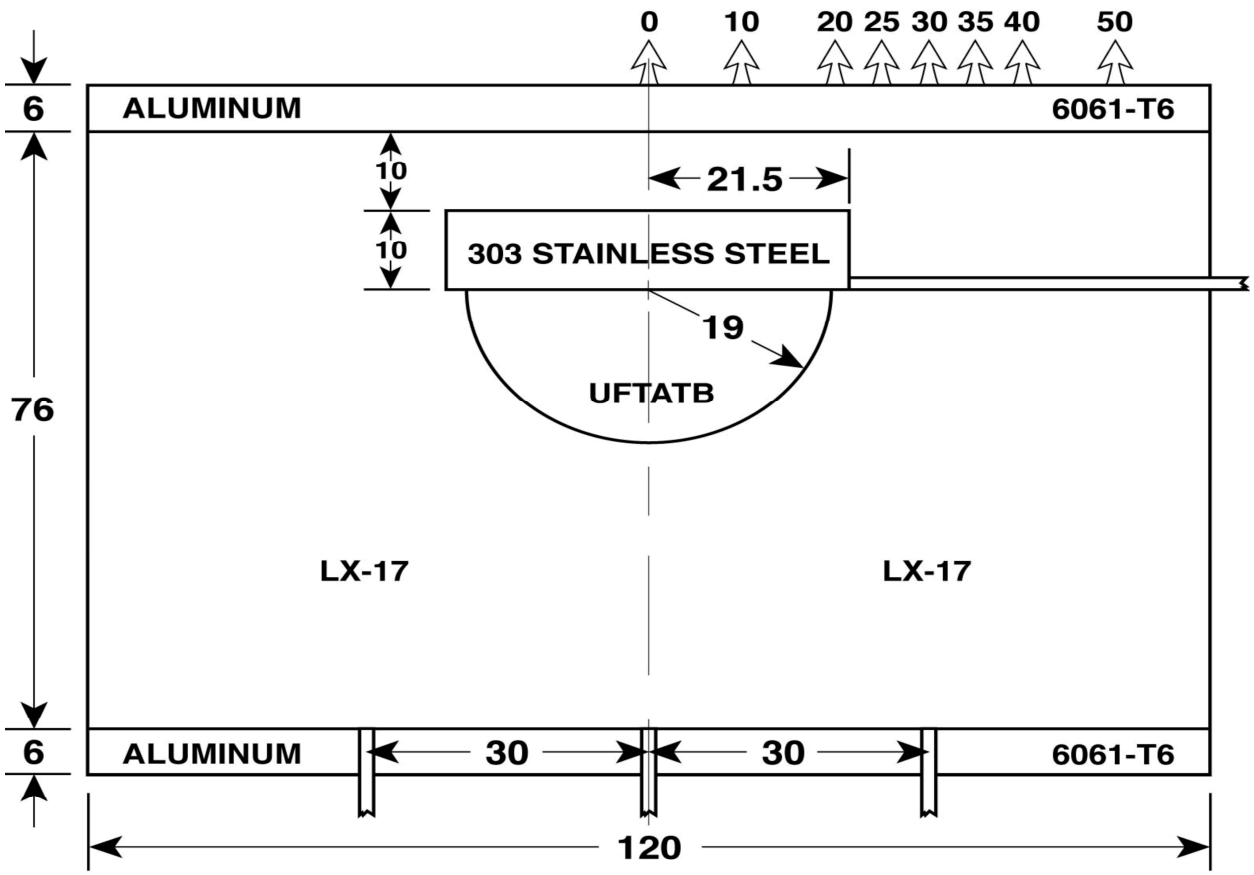

Figure 2. Schematic cross section of experiment E3

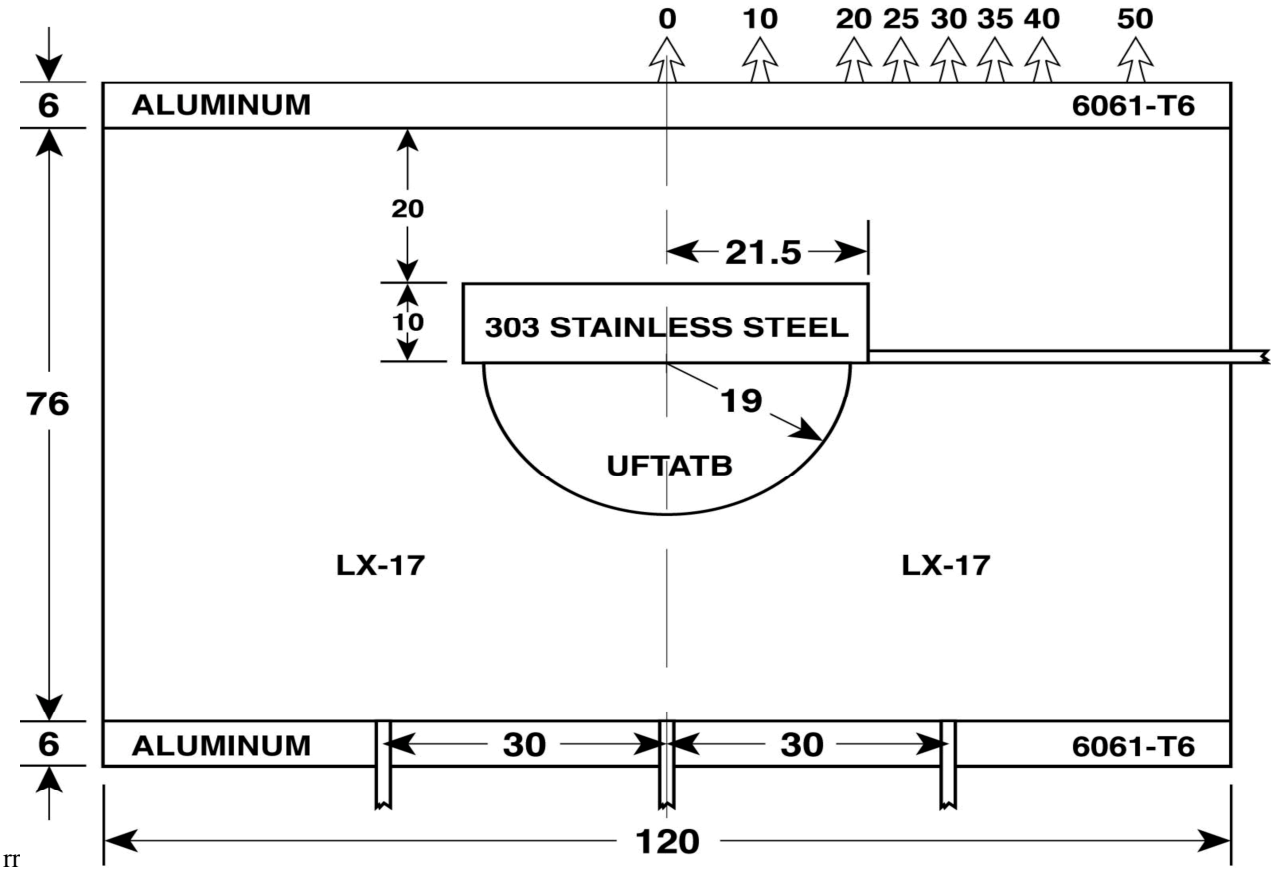

rr

Figure 3. Schematic cross section of experiment E4

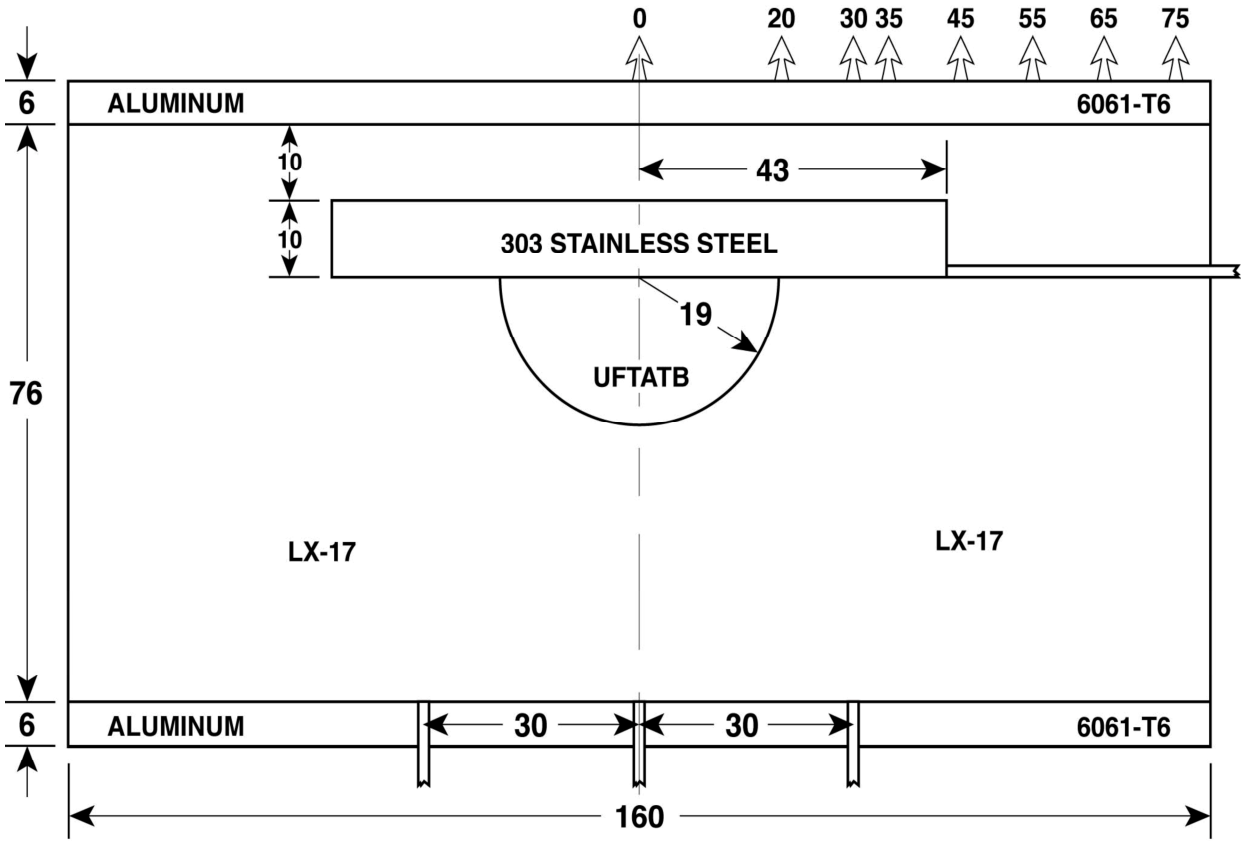

Figure 4. Schematic cross section of experiment E5

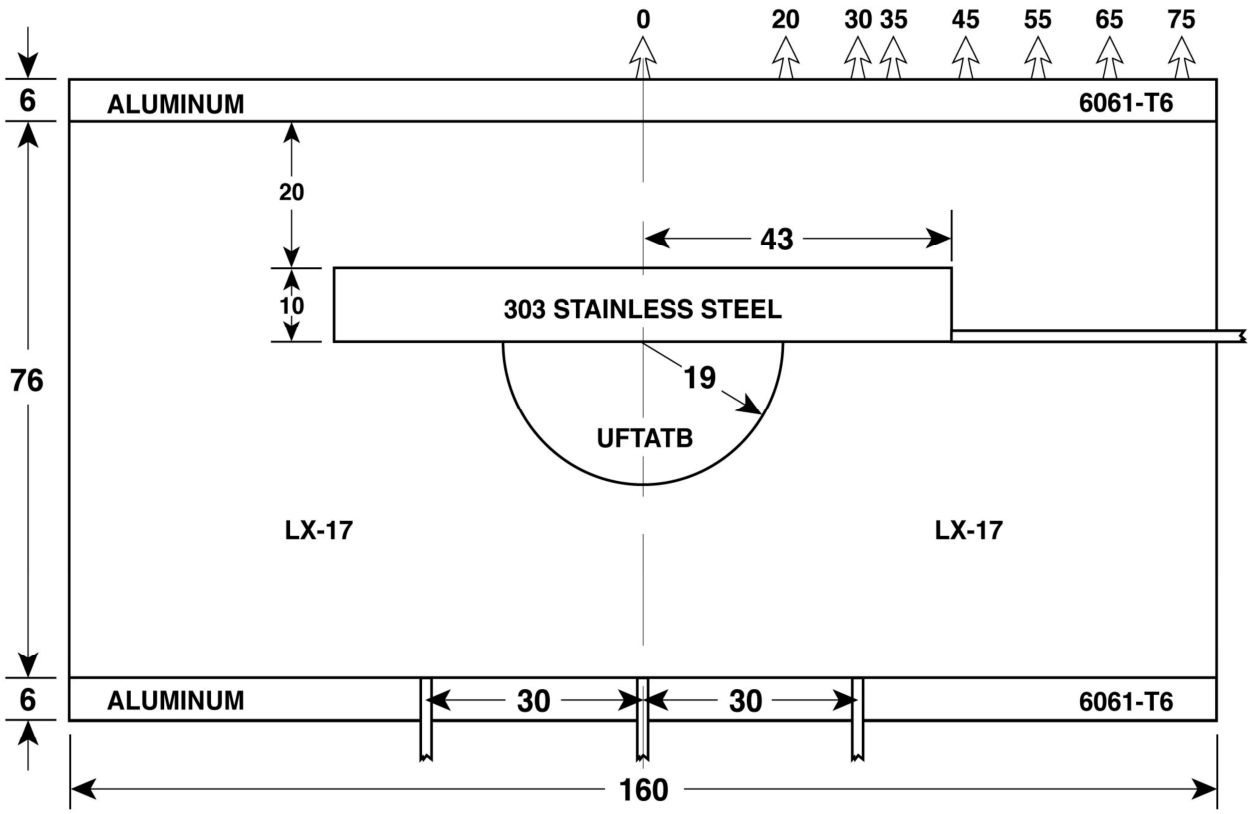

Figure 5. Schematic cross section of experiment E6

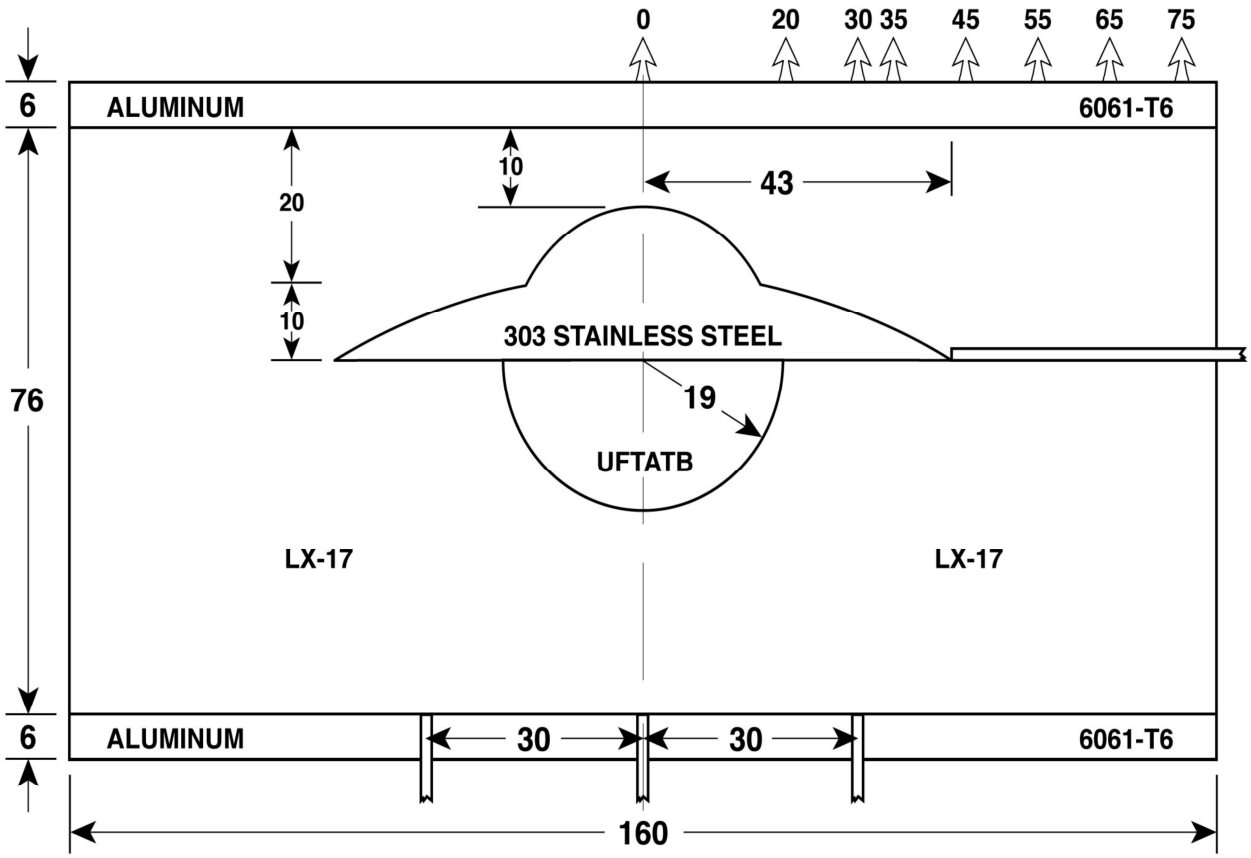

Figure 6. Schematic cross section of experiment E7

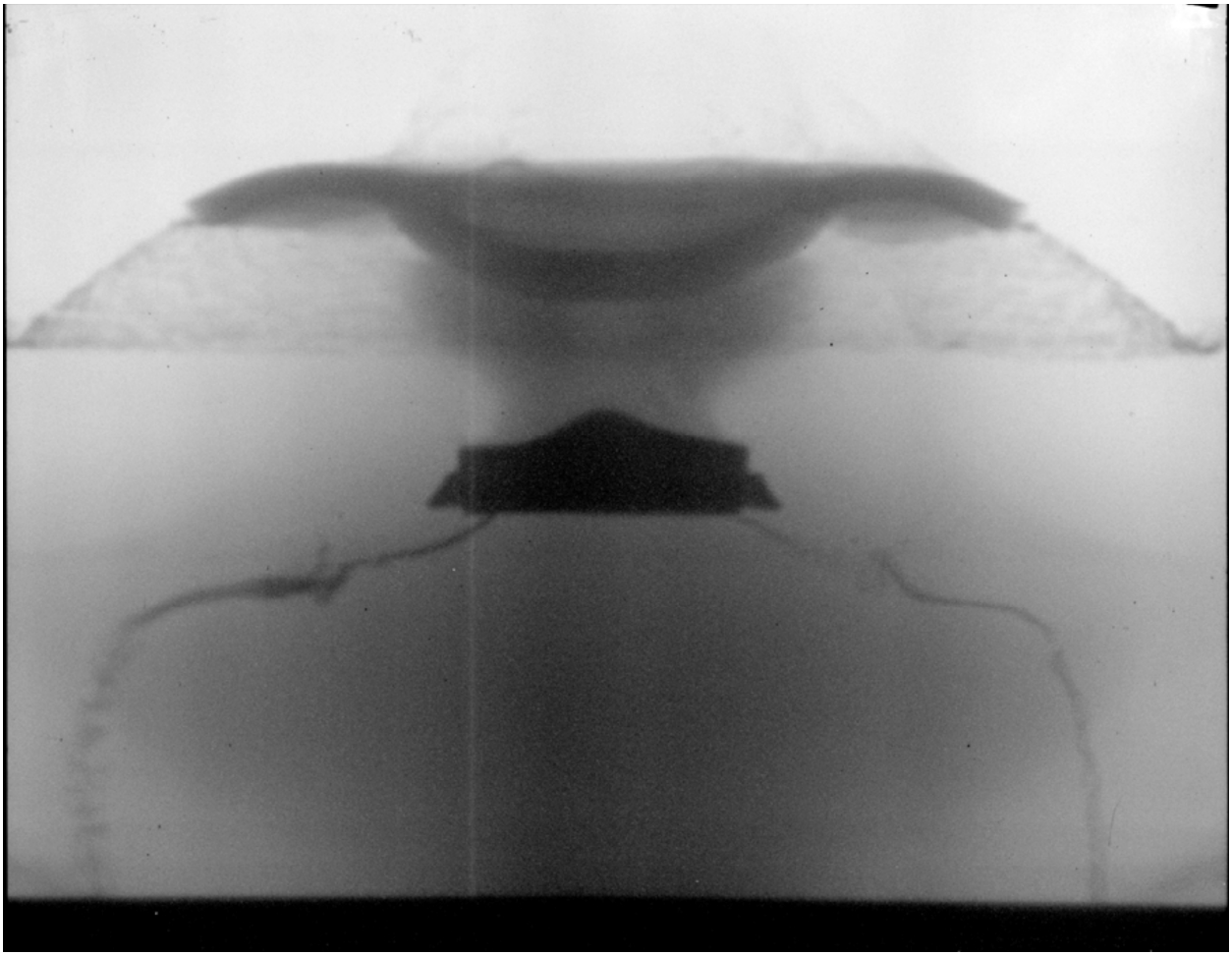

Figure 7. X-ray of experiment E3 taken at 30 microseconds

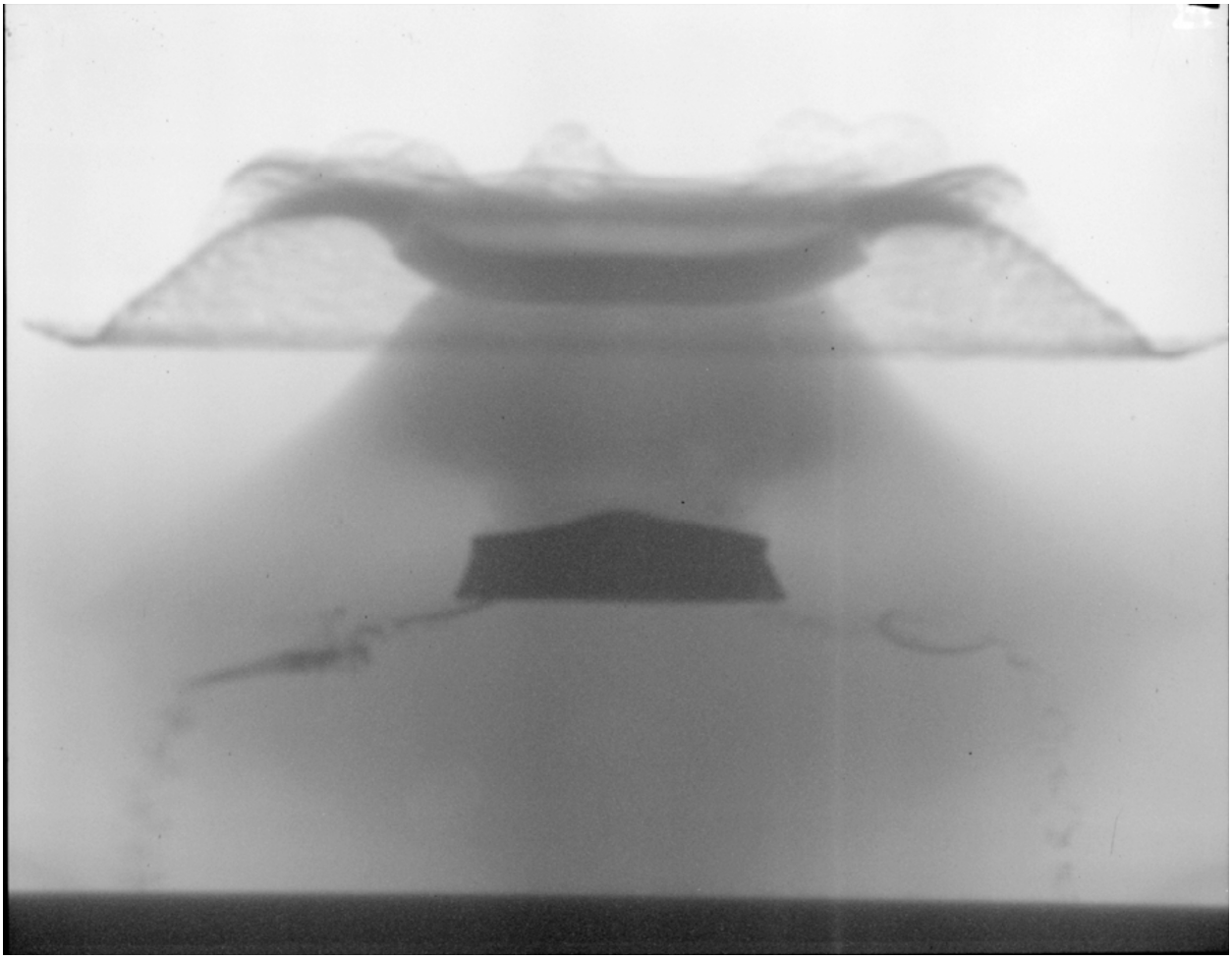

Figure 8. X-ray of experiment E4 taken at 30 microseconds

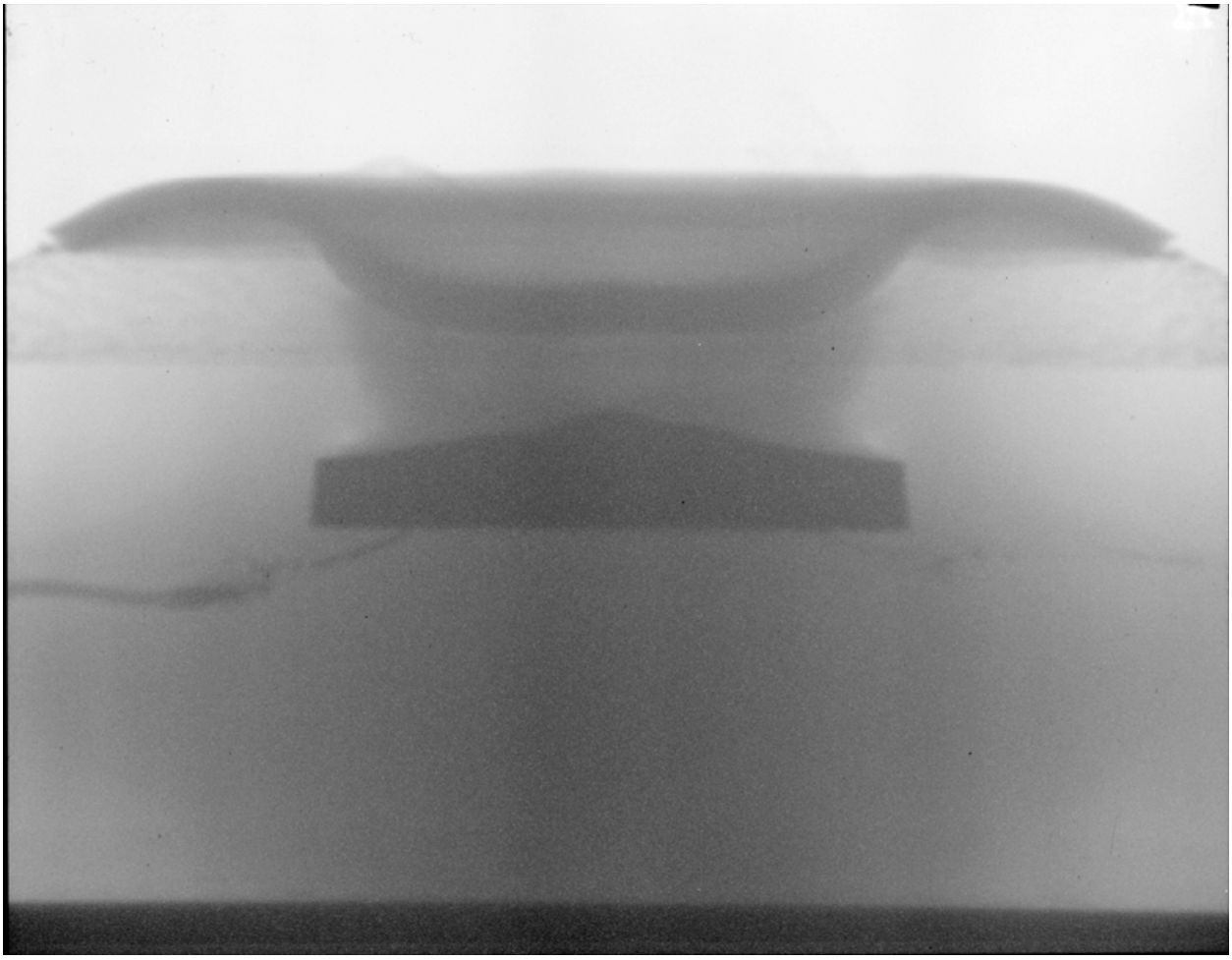

Figure 9. X-ray of experiment E5 taken at 30 microseconds

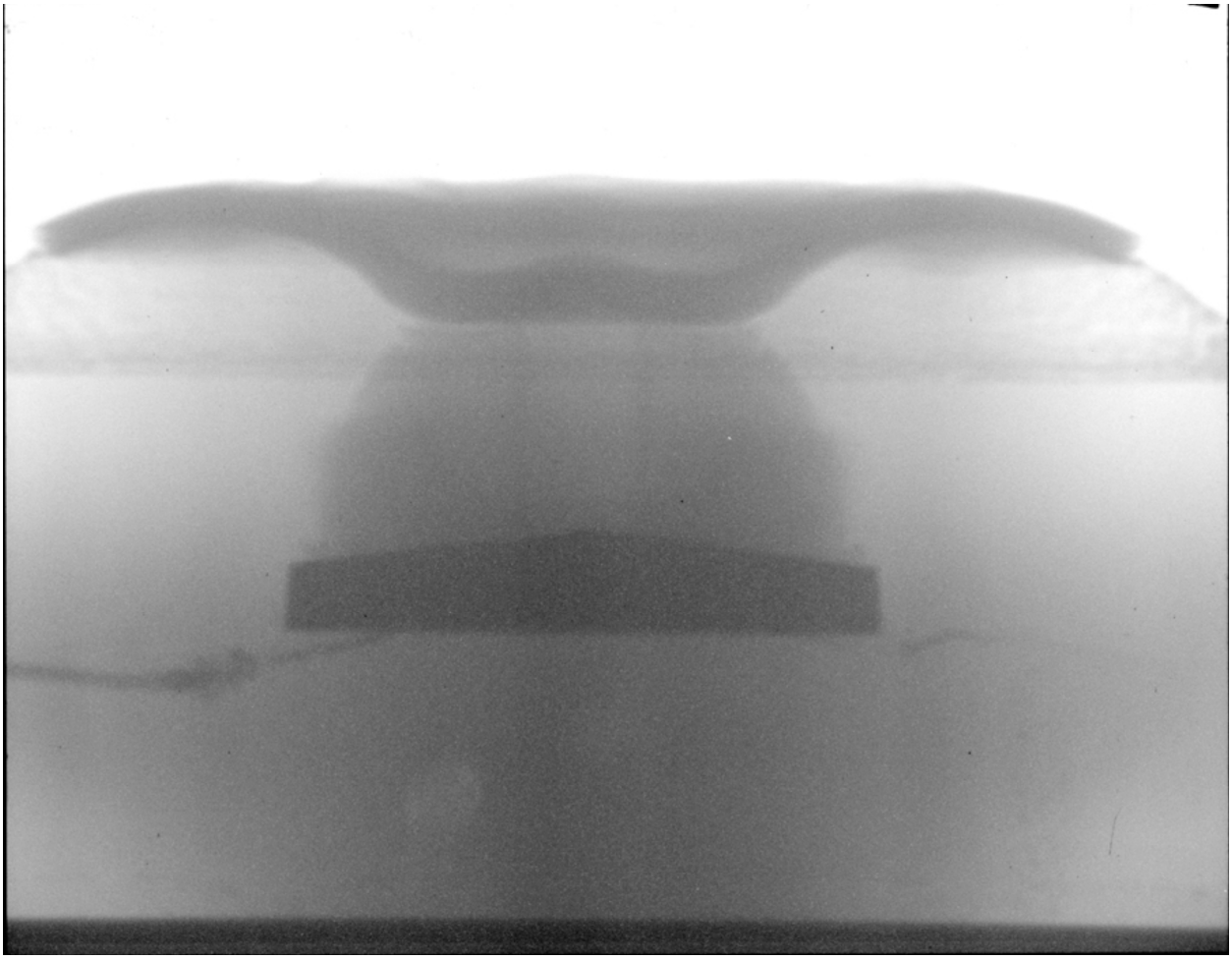

Figure 10. X-ray of experiment E6 taken at 30 microseconds

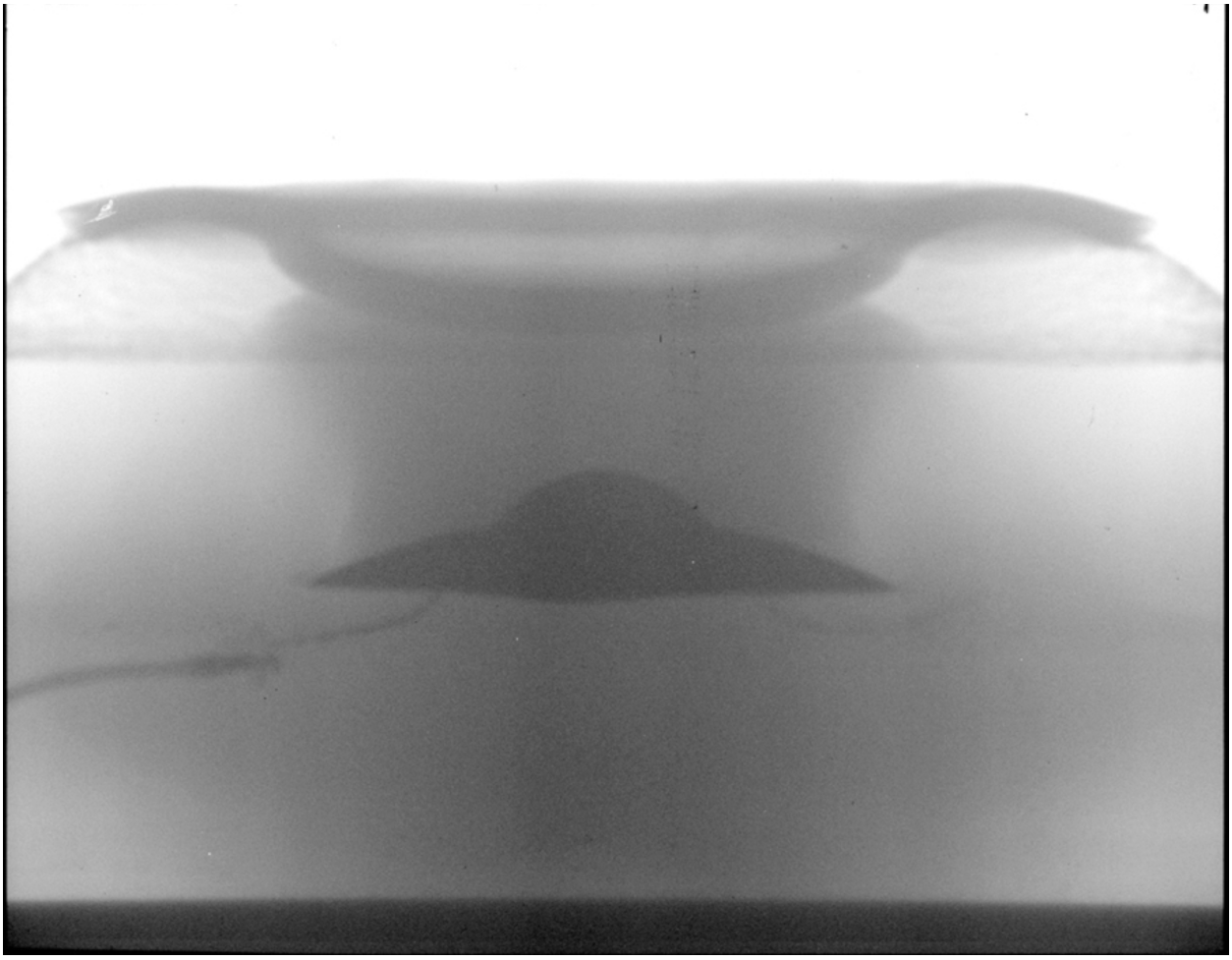

Figure 11. X-ray of experiment E7 taken at 30 microseconds

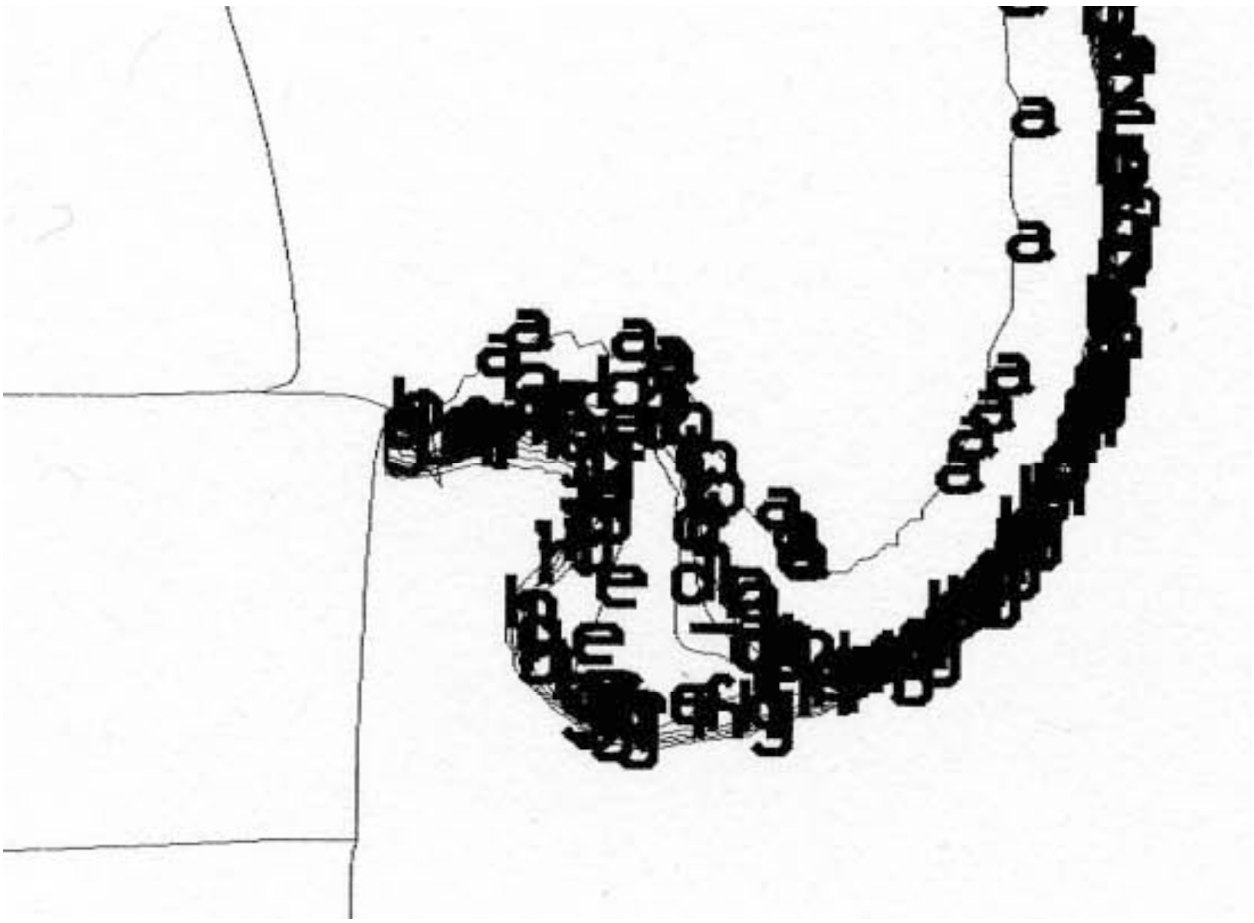

Figure 12. Fraction reacted contours calculated for experiment E3 at 8 μs

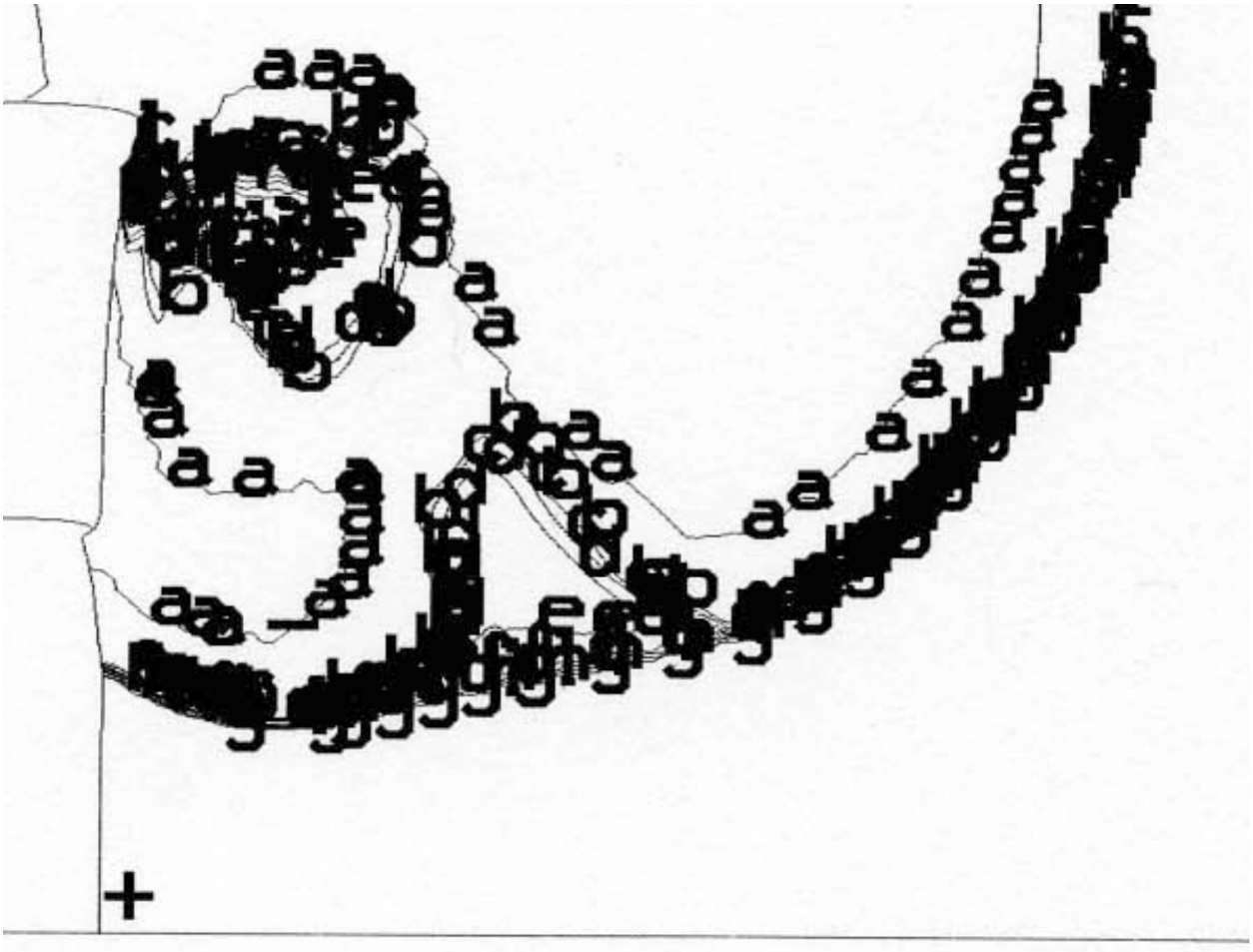

Figure 13. Fraction reacted contours calculated for experiment E3 at 9 μs

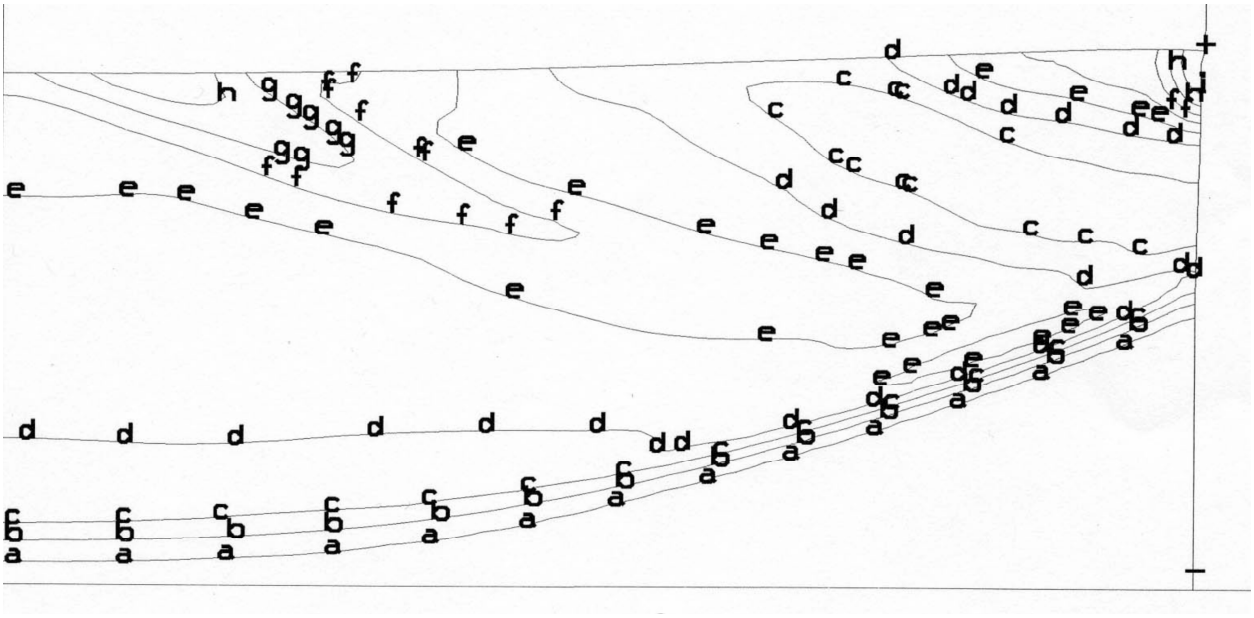

Figure 14. Calculated pressure contours in desensitized LX-17 for experiment E3 at 8.5 μs

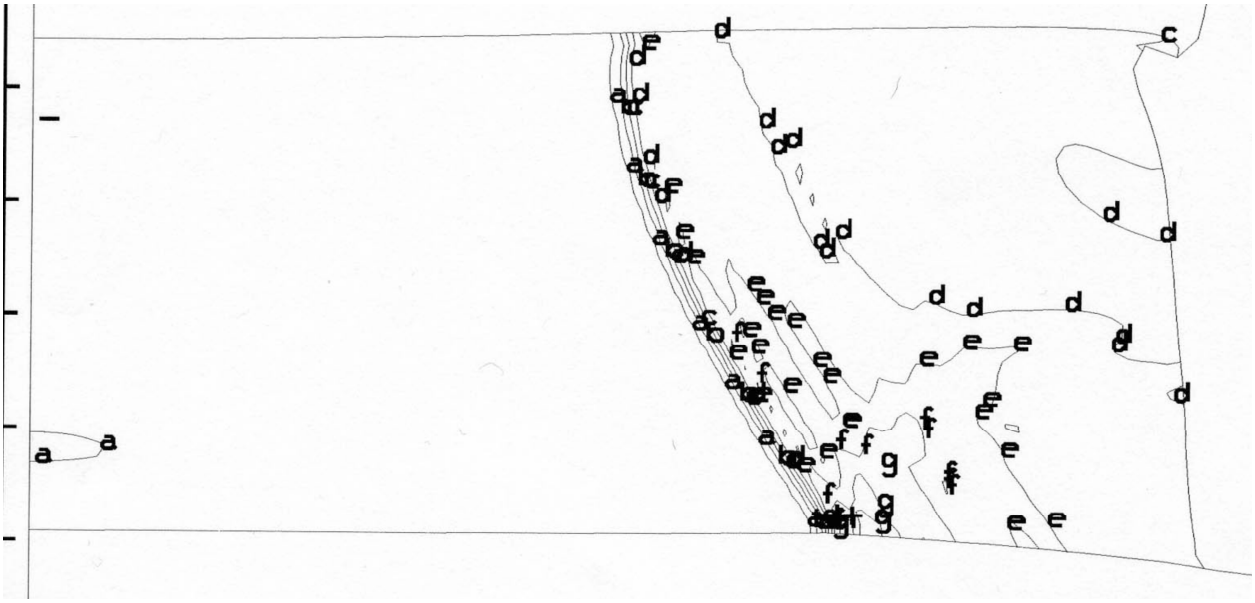

Figure 15. Calculated pressure contours in desensitized LX-17 for experiment E3 at 10.5 μs

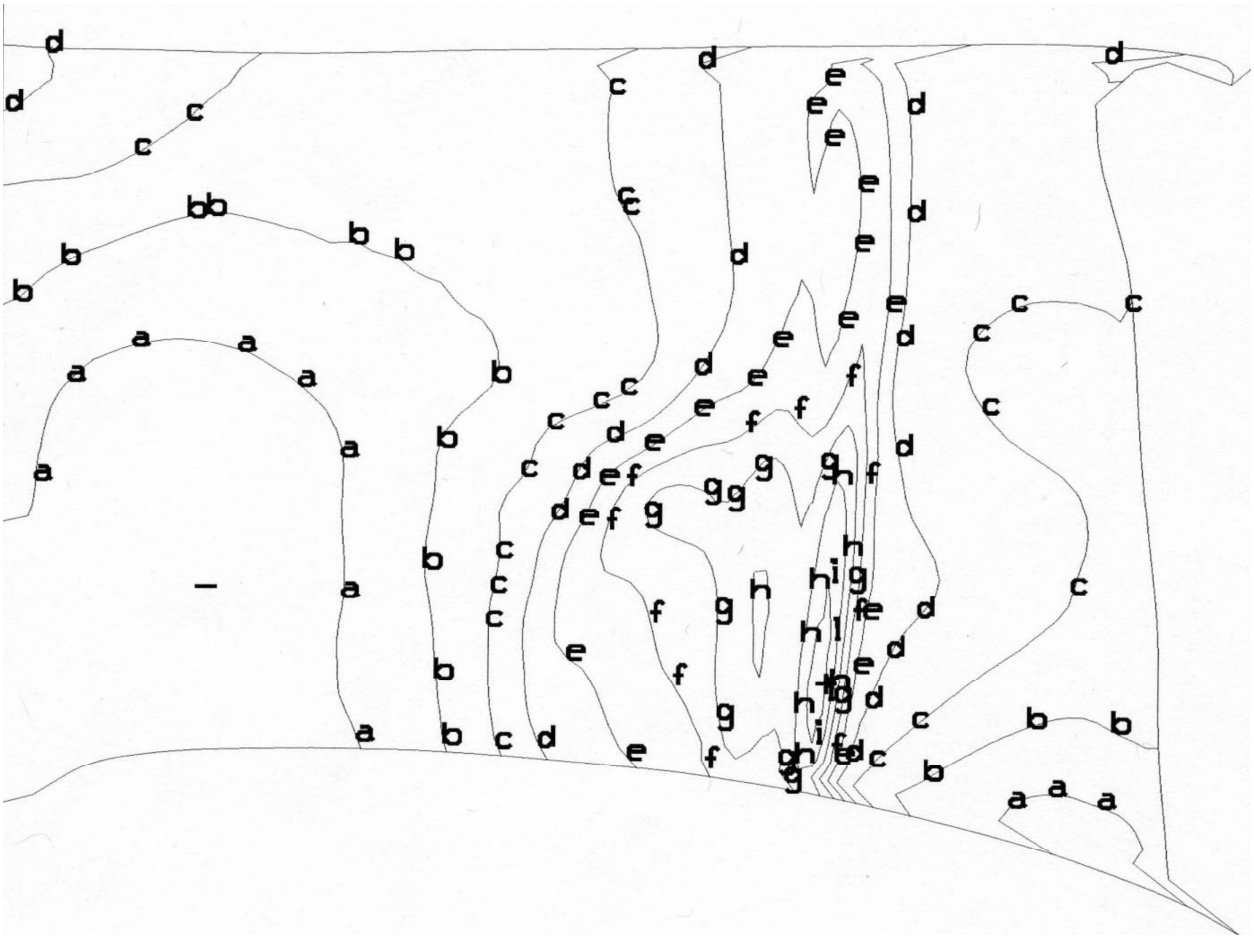

Figure 16. Calculated pressure contours in desensitized LX-17 for experiment E3 at 14.5 μs

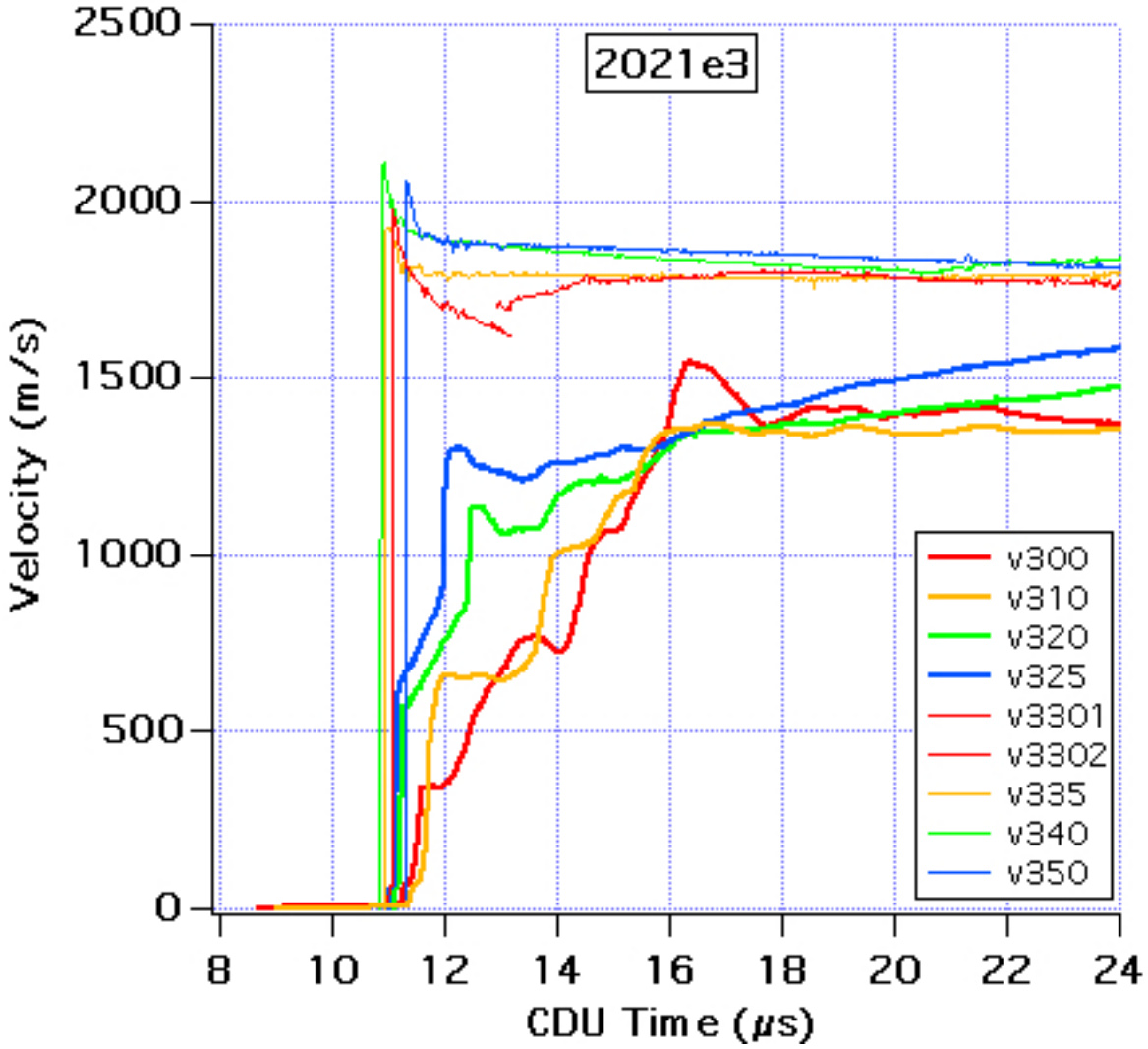

Figure 17. PDV velocity histories measured during experiment E3

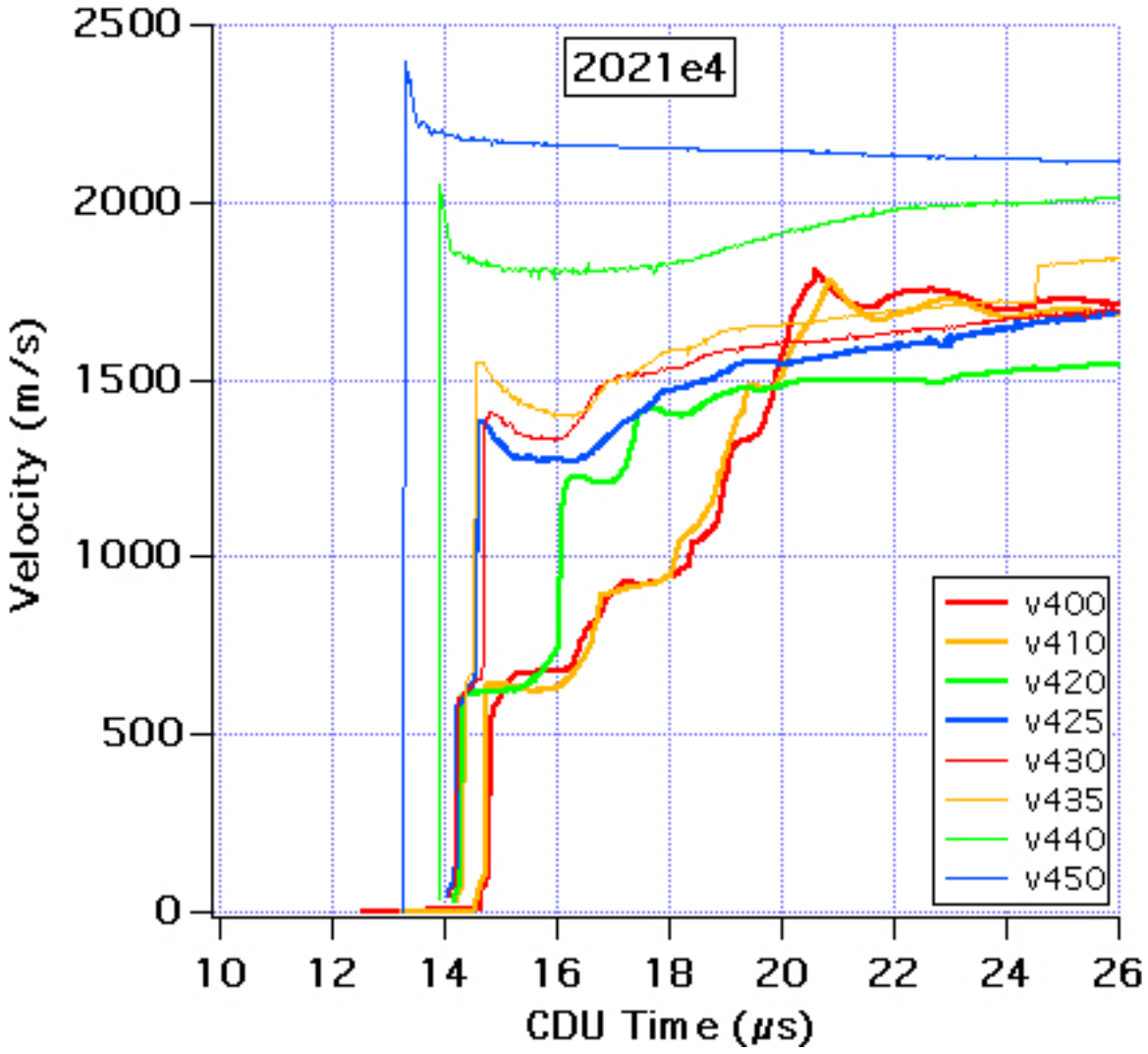

Figure 18. PDV velocity histories measured during experiment E4

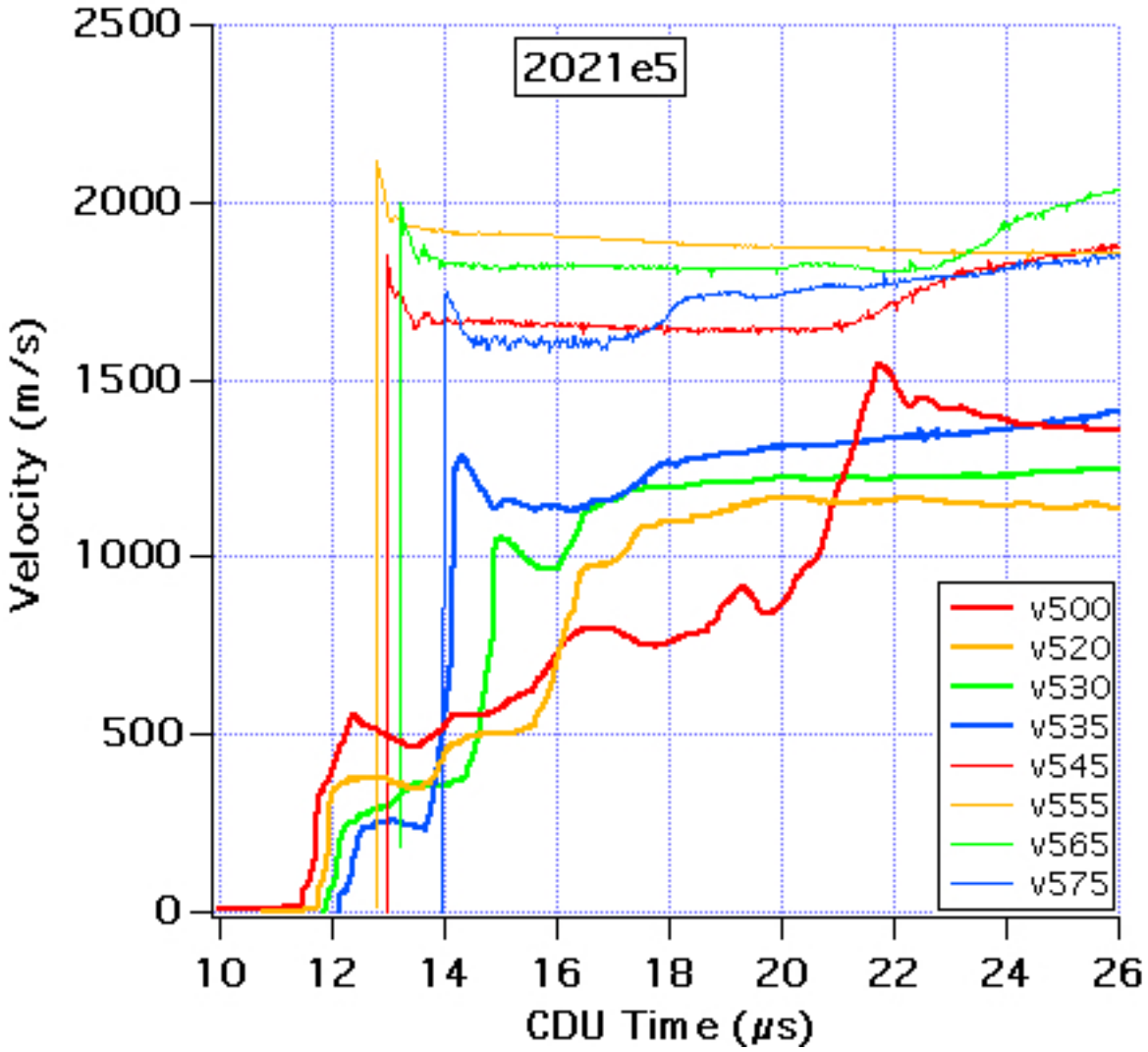

Figure 19. PDV velocity histories measured during experiment E5

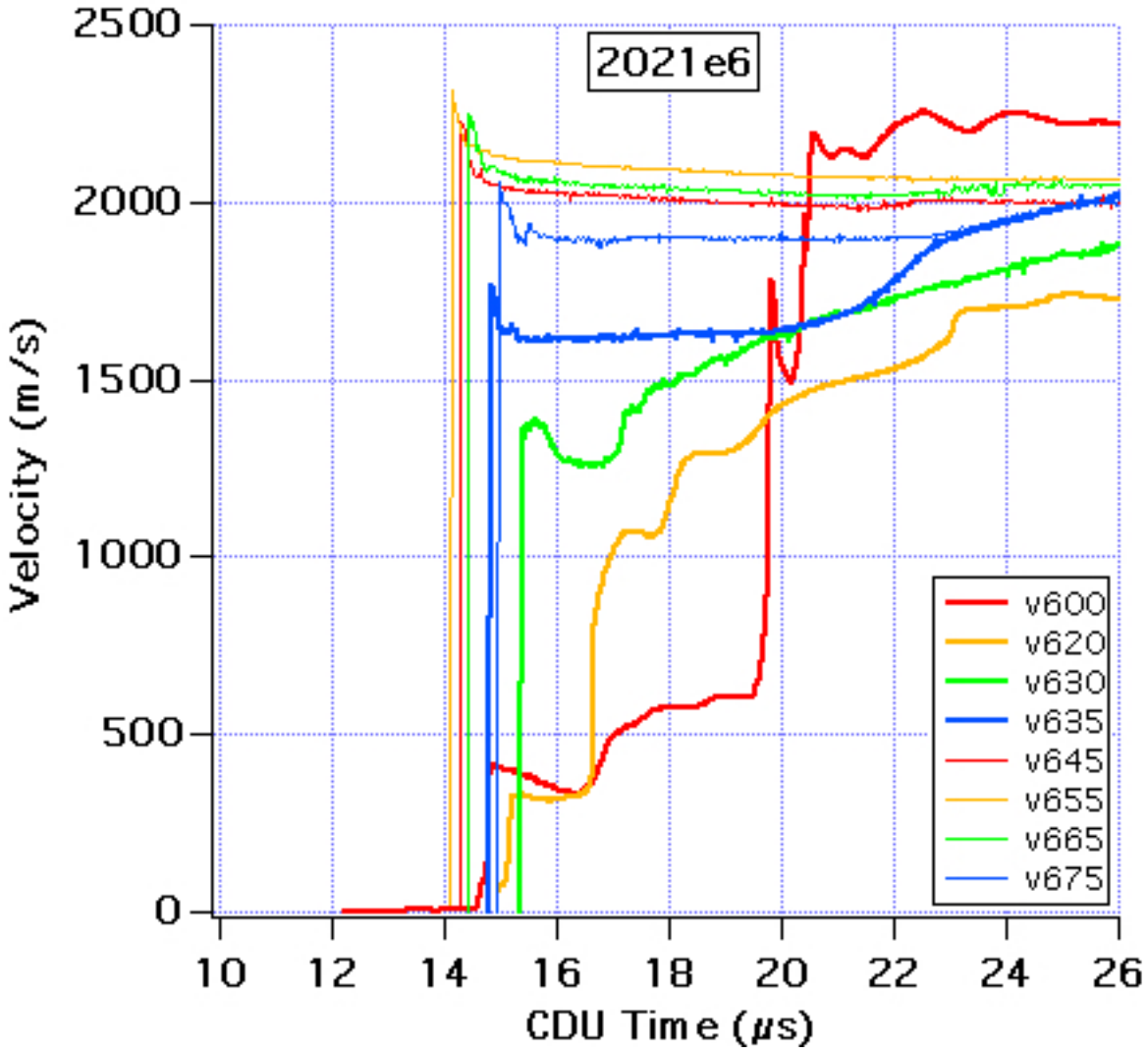

Figure 20. PDV velocity histories measured during experiment E6

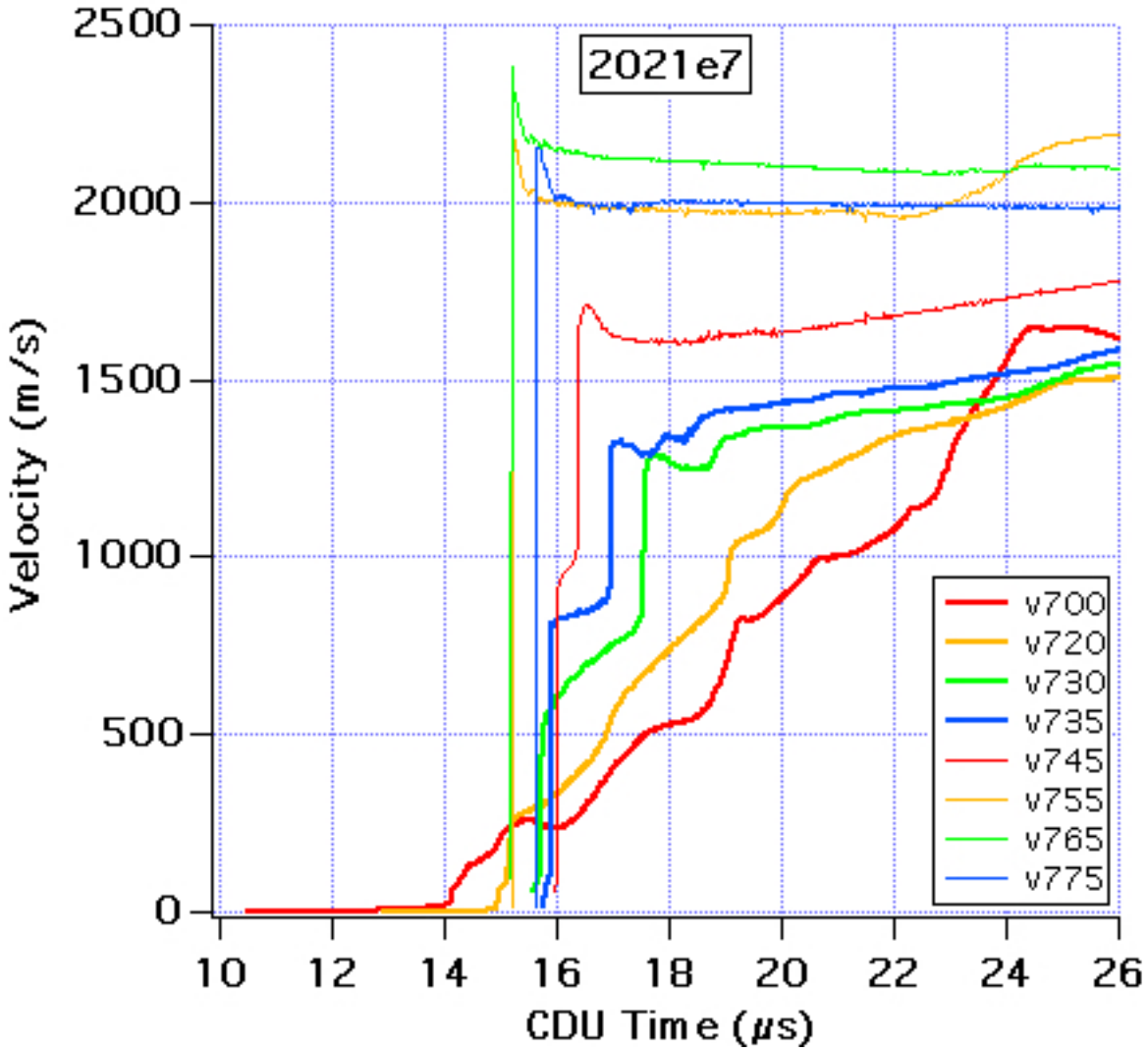

Figure 21. PDV velocity histories measured during experiment E7

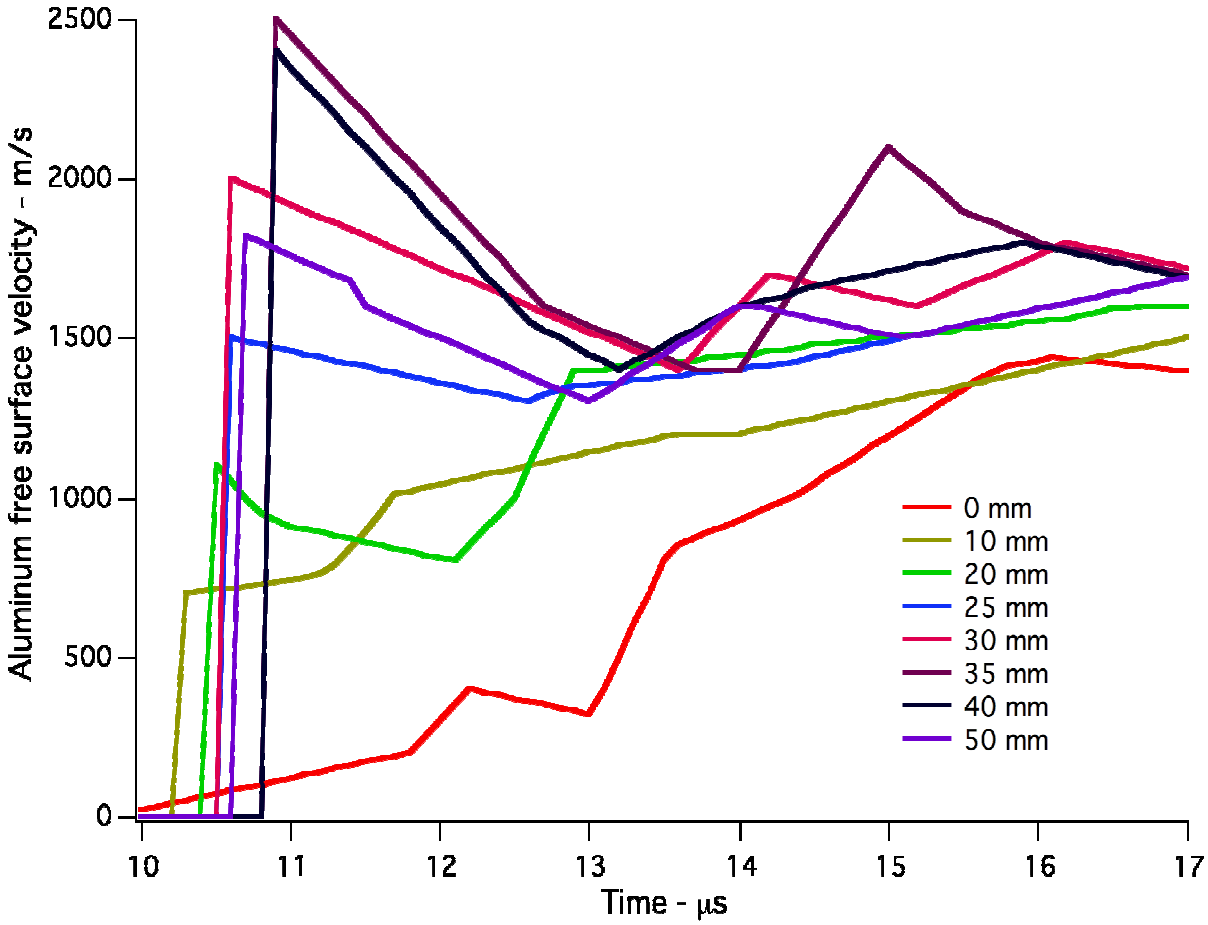

Figure 22. Calculated aluminum plate free surface velocity histories for experiment E3

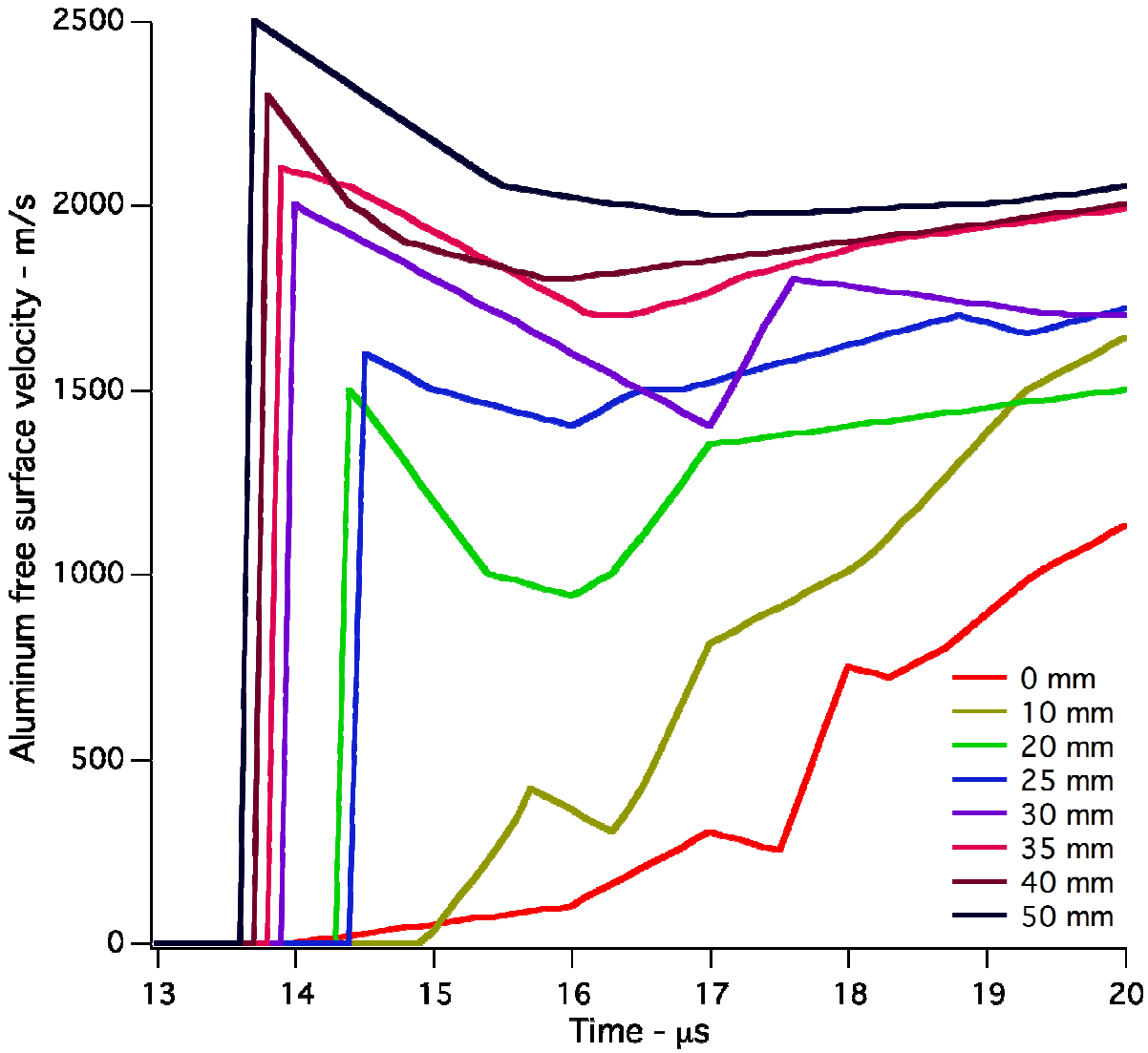

Figure 23. Calculated aluminum free surface velocity histories for experiment E4

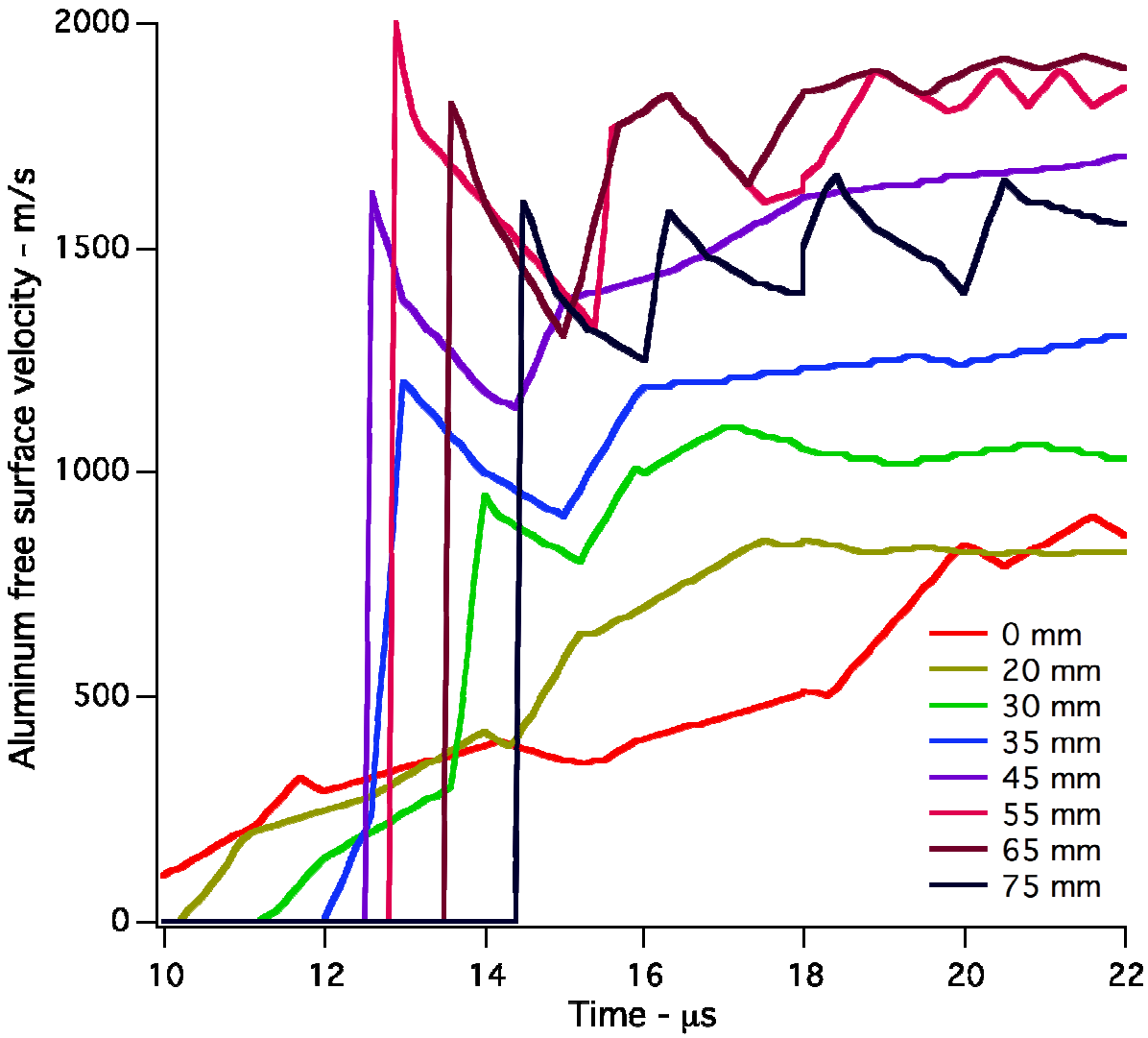

Figure 24. Calculated aluminum free surface velocity histories for experiment E5

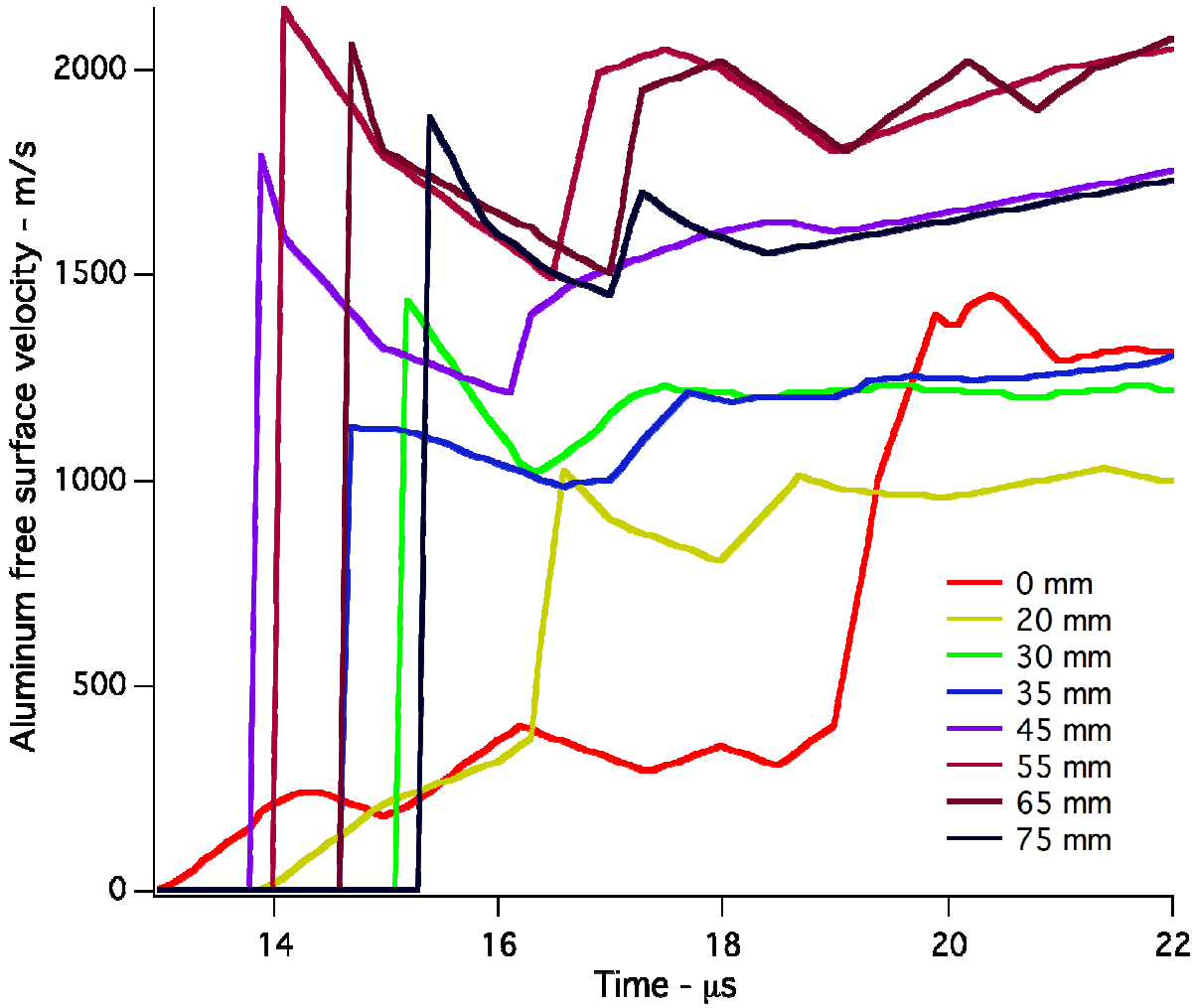

Figure 25. Calculated aluminum free surface velocity histories for experiment E6

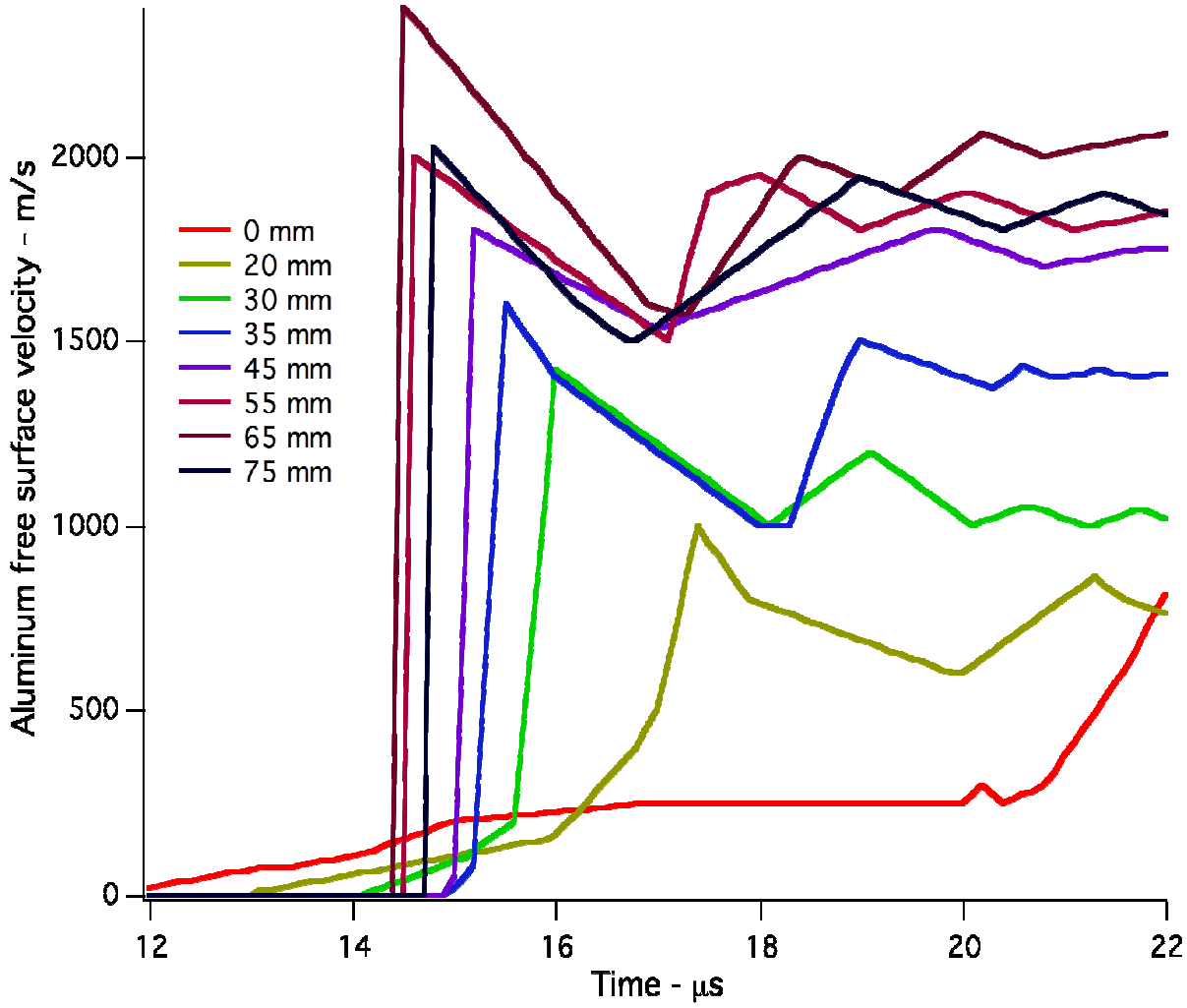

Figure 26. Calculated aluminum free surface velocity histories for experiment E7